



## RESEARCH ARTICLE

10.1002/2017MS001095

## Key Points:

- A diagnostic PDF cloud scheme relating the subgrid-scale variance to turbulence and shallow convection is proposed and tested in CAM5
- The scheme improved the simulation of marine low clouds mainly due to its consideration of subgrid-scale variance
- The improvement is present and the double ITCZ problem is slightly alleviated in preliminary coupled simulation using the new scheme

## Correspondence to:

Y. Lin,  
yanluan@tsinghua.edu.cn

## Citation:

Qin, Y., Lin, Y., Xu, S., Ma, H.-Y., & Xie, S. (2018). A diagnostic PDF cloud scheme to improve subtropical low clouds in NCAR Community Atmosphere Model (CAM5). *Journal of Advances in Modeling Earth Systems*, 10, 320–341.  
<https://doi.org/10.1002/2017MS001095>

Received 19 JUN 2017

Accepted 17 JAN 2018

Accepted article online 22 JAN 2018

Published online 6 FEB 2018

## A Diagnostic PDF Cloud Scheme to Improve Subtropical Low Clouds in NCAR Community Atmosphere Model (CAM5)

Yi Qin<sup>1</sup> , Yanluan Lin<sup>1</sup> , Shiming Xu<sup>1</sup>, Hsi-Yen Ma<sup>2</sup> , and Shaocheng Xie<sup>2</sup>

<sup>1</sup>Ministry of Education Key Laboratory for Earth System Modeling, Department of Earth System Science, and, Joint Center for Global Change Studies, Tsinghua University, Beijing, China, <sup>2</sup>Program for Climate Model Diagnosis and Intercomparison, Lawrence Livermore National Laboratory, Livermore, CA, USA

**Abstract** Low clouds strongly impact the radiation budget of the climate system, but their simulation in most GCMs has remained a challenge, especially over the subtropical stratocumulus region. Assuming a Gaussian distribution for the subgrid-scale total water and liquid water potential temperature, a new statistical cloud scheme is proposed and tested in NCAR Community Atmospheric Model version 5 (CAM5). The subgrid-scale variance is diagnosed from the turbulent and shallow convective processes in CAM5. The approach is able to maintain the consistency between cloud fraction and cloud condensate and thus alleviates the adjustment needed in the default relative humidity-based cloud fraction scheme. Short-term forecast simulations indicate that low cloud fraction and liquid water content, including their diurnal cycle, are improved due to a proper consideration of subgrid-scale variance over the southeastern Pacific Ocean region. Compared with the default cloud scheme, the new approach produced the mean climate reasonably well with improved shortwave cloud forcing (SWCF) due to more reasonable low cloud fraction and liquid water path over regions with predominant low clouds. Meanwhile, the SWCF bias over the tropical land regions is also alleviated. Furthermore, the simulated marine boundary layer clouds with the new approach extend further offshore and agree better with observations. The new approach is able to obtain the top of atmosphere (TOA) radiation balance with a slightly alleviated double ITCZ problem in preliminary coupled simulations. This study implies that a close coupling of cloud processes with other subgrid-scale physical processes is a promising approach to improve cloud simulations.

## 1. Introduction

Clouds play an important role in the planetary energy budget by reflecting and absorbing solar radiation. Low clouds reflect large amount of incoming solar radiation and emit longwave radiation at relatively high temperatures, and thus exert a net cooling effect on the earth (Hartmann, 1994; Klein & Hartmann, 1993). With their extensive distribution and radiative effect, low clouds significantly impact the energy budget, but their simulation in many climate models remains a challenge (Ahlgren & Forbes, 2014; Donner et al., 2011; Lin et al., 2012). Meanwhile, transient and equilibrium climate sensitivity is found to be closely related to the simulation of low clouds (Bony et al., 2015). Bony and Dufresne (2005) revealed that clouds in the subsiding regions are responsible for the large spread of climate sensitivity among GCMs they examined. Therefore, improving low cloud simulation is a critical step toward better model credibility and performance.

Formation and maintenance of low clouds are closely related to multiple processes, such as boundary layer mixing, surface sensible and latent heat fluxes, cloud top radiative cooling, and entrainment (Wood, 2012). Proper representation of these processes and their interactions is necessary in the model to well capture the evolution of low clouds. Previous studies indicated that improving boundary layer top processes, such as the cloud top radiative cooling and entrainment, is critical to the simulation of stratocumulus and the transition between stratocumulus and trade cumulus (Bretherton & Park, 2009; Lock et al., 2000). On the other hand, the coarse vertical grid spacing in the boundary layer also limits the description of cloud top processes, especially the cloud top entrainment layer (Wood, 2012). Increasing the model's vertical resolution is helpful to alleviate the bias of boundary layer cloud simulation to some extent (Bretherton & Park, 2009; Kuwano-Yoshida et al., 2010; Wang et al., 2011). Recently, the unified turbulence and cloud parameterization based on multivariate probability density function was found to capture more realistic boundary layer processes with improved simulation of stratocumulus (Bogenschutz et al., 2012, 2013; Cheng & Xu, 2015; Guo et al., 2014).

© 2018. The Authors.

This is an open access article under the terms of the Creative Commons Attribution-NonCommercial-NoDerivs License, which permits use and distribution in any medium, provided the original work is properly cited, the use is non-commercial and no modifications or adaptations are made.

A relative humidity (RH)-based cloud scheme was first proposed by Sundqvist et al. (1989), who related the cloud fraction to the grid mean RH with diagnosed condensation rates. Due to their simplicity, RH schemes are still widely used in many GCMs (Schmidt et al., 2006; Scinocca et al., 2008; Stevens et al., 2013). RH-based cloud schemes diagnose the cloud fraction from the grid mean RH, but the condensation needs to be diagnosed or prognosed via other methods (Park et al., 2014; Sundqvist et al., 1989; Zhang et al., 2003). Moreover, the selection of RH threshold is generally empirical, and it is often used as a tuning parameter during the model development (Hourdin et al., 2017; Kay et al., 2016; Mauritsen et al., 2012). However, cloud fraction and cloud feedback are sensitive to the choice of the RH threshold (Quaas, 2012). Hence, using the RH threshold introduces uncertainties to the simulation of current climate and climate projections. The Tiedtke scheme (Tiedtke, 1993) is often regarded as the archetype of prognostic cloud scheme. It predicts the cloud fraction by directly including effects from other related physical processes, such as turbulent mixing, convection, and others. The prognostic cloud scheme prognoses cloud fraction and cloud water at the same time, but complex physical processes involved make it difficult to exactly identify the processes leading to the improvement of clouds. Overall, since cloud fraction and condensation are handled separately via different procedures, these two methods tend to have inconsistencies between cloud fraction and cloud condensate (Gregory et al., 2002; Park et al., 2014; Tompkins, 2005; Zhang et al., 2003).

Statistical cloud schemes assume a subgrid-scale probability distribution function (PDF) of total water specific humidity, saturation deficit, or a combined variable of liquid water potential temperature and total water specific humidity to determine the cloud fraction and condensation (Bougeault, 1981; Kuwano-Yoshida et al., 2010; Mellor, 1977; Smith, 1990; Sommeria & Deardorff, 1977). Assuming specific PDFs with their moments diagnosed or prognosed, integration of the PDFs will give the cloud fraction and condensate consistently. The key for statistical cloud schemes is to determine the PDF form and their moments. Because of the complexity of clouds in reality and limited observations, various PDF distributions have been explored, including Gaussian (Mellor, 1977; Sommeria & Deardorff, 1977), triangular (Smith, 1990), beta (Tompkins, 2002), lognormal (Bony & Emanuel, 2001), gamma (Bougeault, 1982), and Double-Gaussian distribution (Golaz et al., 2002; Lewellen & Yoh, 1993; Luhar et al., 1996; Naumann et al., 2013). Previous studies indicate that relating the PDF moments to other physical processes is a promising way to improve cloud simulations (Bechtold et al., 1992; Bougeault, 1981; Kuwano-Yoshida et al., 2010). In addition to those “pure” diagnostic statistical cloud schemes (Bechtold et al., 1992; Bougeault, 1981, 1982; Kuwano-Yoshida et al., 2010), some hybrid statistical cloud schemes with prognosed PDF moments have been explored with promising results (Tompkins, 2002; Watanabe et al., 2009).

Large low cloud biases remained in CAM5, especially regarding the sharp transition from coastal stratocumulus to offshore shallow cumulus over the subtropical ocean regions (Hannay et al., 2009; Park et al., 2014; Xiao et al., 2014). The sharp transition might be caused by the tendency for decoupled boundary layers during the daytime (Medeiros et al., 2012) or overactive shallow convection (Xiao et al., 2014). A close connection among boundary layer turbulence, shallow convection, and cloud scheme might be a way to reduce those biases. Our goal here is to design a relatively simple and efficient PDF cloud scheme closely related to the boundary layer and shallow convection schemes to improve subtropical low cloud simulation in CAM5.

This paper introduces a Gaussian PDF cloud scheme with the PDF variance diagnosed from the turbulent and shallow convective processes. Section 2 describes the new scheme and its main differences from the default cloud scheme. Evaluation of the scheme using global short-term hindcast simulations is in section 3. Climate simulation results using the new approach are presented in section 4 with some preliminary results from a short-coupled simulation. Discussion and conclusions are presented in section 5.

## 2. Diagnostic PDF Cloud Scheme and Its Implementation in CAM5

Cloud types are separated into two categories in CAM5: stratiform clouds (liquid and ice stratiform clouds) and convective clouds (deep convective and shallow convective clouds). The liquid and ice stratiform clouds are diagnosed using the Park macrophysical scheme, and convective clouds are related to deep and shallow convection schemes (Neale et al., 2012; Park et al., 2014).

The default cloud macrophysical scheme in CAM5 (called as Park-RH scheme hereafter) includes diagnostic stratiform cloud fractions and a prognostic large-scale condensation (Neale et al., 2012). Liquid stratiform clouds are diagnosed based on a symmetric triangular PDF of total water RH and a critical RH varying with altitudes and surface properties (Park et al., 2014). The width of PDF only depends on the critical RH, which

generally decreases with heights because of the larger subgrid-scale variance in the upper levels (Quaas, 2012). The calculation of large-scale condensation follows Zhang et al. (2003) with refinements to obtain the consistency with the cloud structures in CAM5 (Park et al., 2014). Although the diagnostic stratiform cloud fraction is directly used for the calculation of net condensation, inconsistency between cloud fraction and condensate is present in this approach. Occurrence of “empty” or “dense” clouds makes the adjustment between cloud fraction and condensate necessary (Park et al., 2014).

In order to alleviate the inconsistency between cloud fraction and condensate, we introduce the Gaussian PDF statistical cloud scheme (called as Gauss-PDF hereafter). Based on observations, Lin (2014) found that assuming a Gaussian PDF is able to derive cloud fraction realistically given that the subgrid-scale variance is well known. For simplicity, we assume a Gaussian distribution for the subgrid variation of total water and liquid water potential temperature following Sommeria and Deardorff (1977) and Mellor (1977). The prognostic large-scale condensation in Park-RH (Zhang et al., 2003) is replaced by a diagnosed condensation directly from Gauss-PDF, and the diagnostic cloud fraction from Gauss-PDF represents the liquid stratiform clouds and shallow convective clouds in Park-RH as one cloud type. Deep convective clouds and ice stratiform clouds are handled similarly as in CAM5. Overall, we replace the default Park-RH scheme by the Gauss-PDF scheme with other physical processes identical as those in CAM5.

Gauss-PDF is based on the statistical cloud scheme proposed by Sommeria and Deardorff (1977) and Mellor (1977). Liquid water potential temperature ( $\theta_l = \theta - \frac{L\theta}{c_p T} q_l$ ) and total water specific humidity ( $q_w = q_v + q_l$ ) are the basic variables. Since perturbations from water vapor and temperature affect saturated water vapor pressure and further influence the condensate, the joint PDF of  $q_w$  and  $\theta_l$  can be expressed by a single variable  $s$  after some algebra:

$$s = \frac{aq'_w - b\theta'_l}{2} \quad (1)$$

with

$$a = (1 + L\bar{q}_{sl,T}/c_p)^{-1}$$

$$b = \frac{\bar{T}}{\bar{\theta}} \frac{\bar{q}_{sl,T}}{1 + L\bar{q}_{sl,T}/c_p}$$

$$q_{sl,T} = \left. \frac{\partial q_s}{\partial T} \right|_{T=T_l} = \frac{0.622Lq_{sl}}{R_d T_l^2}$$

$$q_{sl} = q_s(T_l, p) = \frac{0.622e_s(T_l)}{p - 0.378e_s(T_l)}$$

The overbar denotes the grid mean value and the prime represents the deviation from the mean state.  $T$  is temperature,  $p$  is pressure,  $T_l$  is liquid water temperature,  $\theta$  is potential temperature,  $q_v$  is water vapor specific humidity,  $q_l$  is liquid water specific humidity,  $q_s$  is saturated specific humidity,  $L$  is evaporative latent heat,  $R_d$  is the gas constant of dry air, and  $c_p$  is the specific heat capacity at constant pressure.

Assuming that the normalized “ $s$ ” follows a Gaussian PDF, we get the expression of cloud fraction ( $R$ ) and cloud condensate ( $q_l$ ) as

$$R = \frac{1}{2} \left( 1 + \text{erf} \left( \frac{Q_1}{\sqrt{2}} \right) \right) \quad (2)$$

$$\frac{q_l}{2\sigma_s} = Q_1 R + \frac{e^{-\frac{Q_1^2}{2}}}{\sqrt{2\pi}} \quad (3)$$

in which  $Q_1 = a\Delta\bar{q}/(2\sigma_s) = a(\bar{q}_w - \bar{q}_{sl})/(2\sigma_s)$  is a dimensionless variable describing the departure of the mean state from saturation.

The variance of  $s$  is

$$\sigma_s^2 = \frac{1}{4} \left( a^2 \overline{q'_w}^2 + b^2 \overline{\theta'_l}^2 - 2ab \overline{q'_w \theta'_l} \right) \quad (4)$$

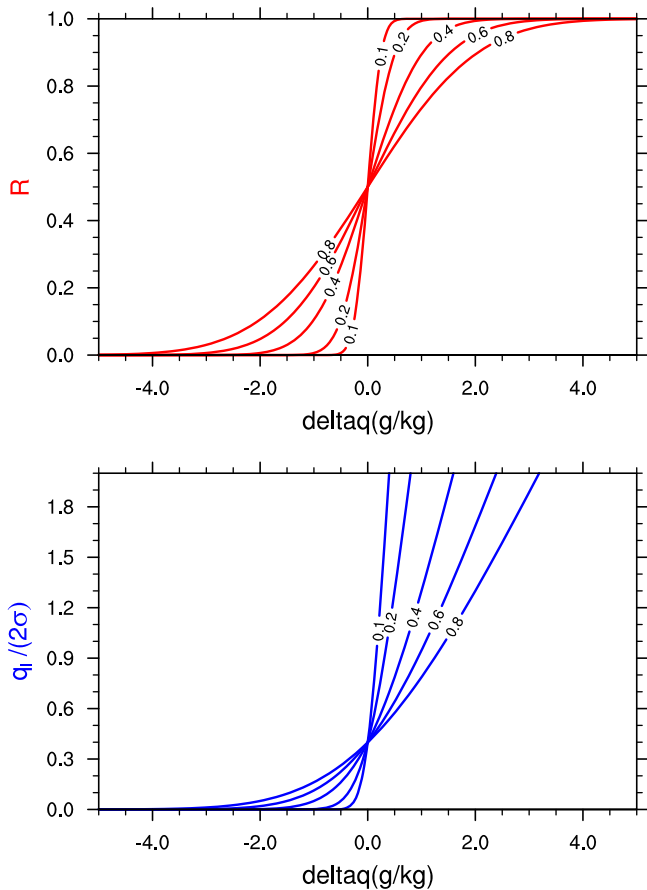


**Figure 1.** The relation between (a) cloud fraction  $R$ , (b) liquid water  $q_l/(2\sigma)$ , and saturation deficit ( $\Delta q$ ; g kg $^{-1}$ ) under different subgrid-scale standard deviations.

Cloud fraction and condensate in this approach (equations (2) and (3)) are determined by  $Q_1$ , which is mainly controlled by the saturation deficit ( $\Delta \bar{q}$ ) and subgrid-scale variance of “ $s$ ” ( $\sigma_s^2$ ). The close relationship between cloud fraction/condensate and subgrid-scale variance is shown in Figure 1. Obviously, the cloud fraction is limited by 0.5 and 1 under unsaturated ( $\Delta \bar{q} < 0$ ) and saturated ( $\Delta \bar{q} > 0$ ) situations, respectively. Increased subgrid-scale variance leads to increased cloud fraction and condensate with a fixed negative saturation deficit, but it causes decreased cloud fraction and condensate with a fixed positive saturation deficit. The increased subgrid-scale variance increases the inhomogeneous distribution of total water when the grid mean is unsaturated. It is beneficial to the cloud formation because it increases the possibility to have subgrid-scale saturation in the grid box. Cloud fraction approaches one when subgrid-scale variance is negligible under the saturated situation.

As discussed above, the key is to determine the subgrid-scale variance, which is closely connected to other physical processes. For simplification, we first include the subgrid-scale variances from turbulence ( $\sigma_{st}^2$ ) and shallow convection ( $\sigma_{ss}^2$ ):

$$\sigma_s^2 = \sigma_{st}^2 + \sigma_{ss}^2 \quad (5)$$

Note that the total water is not conserved for the deep convection because of the existence of large precipitation. Hence, the approximate balance between production and dissipation term in variance budget equation (A2) is no longer valid here because the precipitation and convective detrainment need to be considered. Therefore, Gauss-PDF mainly aims to deal with low clouds with negligible precipitation.

According to the tendency equation of the covariance between total water and liquid potential temperature (A1) and the approximate balance between the production and dissipation term, the subgrid-scale variance caused by turbulence ( $\sigma_{st}^2$ ) is expressed as

$$\sigma_{st}^2 = c_1 S_h I^2 \left( a^2 \left( \frac{\partial q_w}{\partial z} \right)^2 + b^2 \left( \frac{\partial \theta_l}{\partial z} \right)^2 - 2ab \frac{\partial q_w}{\partial z} \frac{\partial \theta_l}{\partial z} \right) \quad (6)$$

where  $c_1$  is a constant of 3.57,  $I$  is the turbulence length scale, and  $S_h$  is the nondimensional stability function from the moist turbulence scheme (Bretherton & Park, 2009).

Similarly, based on the balance between production and dissipation term and using the mass flux in the shallow convection scheme (Park & Bretherton, 2009) to parameterize the corresponding turbulent fluxes in the production term, we get the subgrid-scale variance from shallow convection ( $\sigma_{ss}^2$ ) as

$$\sigma_{ss}^2 = -\frac{1}{2} M_{scu} \frac{I_{clu}}{w^*} * \left\{ a^2 (q_{w,u} - \bar{q}_w) \frac{\partial \bar{q}_w}{\partial z} + b^2 (\theta_{l,u} - \bar{\theta}_l) \frac{\partial \bar{\theta}_l}{\partial z} - ab \left[ (\theta_{l,u} - \bar{\theta}_l) \frac{\partial \bar{q}_w}{\partial z} + (q_{w,u} - \bar{q}_w) \frac{\partial \bar{\theta}_l}{\partial z} \right] \right\} \quad (7)$$

where  $M_{scu}$  is the shallow convective mass flux with the unit of m s $^{-1}$ ,  $I_{clu}$  is the convective cloud depth,  $w^*$  is the convective velocity scale in the boundary layer, the subscript  $u$  is used to denote the updraft quantity and the overbar indicates the grid mean quantity. Detailed calculation of the updraft quantities is in Neale et al. (2012).

The cloud water tendency from the large-scale condensation is directly calculated at each time step in Park-RH. In contrast, the large-scale condensation is indirectly derived from the diagnosed condensate in Gauss-PDF. Gauss-PDF operates on the updated state after the deep and shallow convection. The input temperature ( $T^0$ ), water vapor specific humidity ( $q_v^0$ ), and liquid water specific humidity ( $q_l^0$ ) are used to diagnose the new cloud fraction ( $R^1$ ) and cloud water ( $q_l^1$ ), which are then used to update  $T^0$  and  $q_v^0$ . Liquid water tendency, i.e., large-scale condensation, is the difference between  $q_l^1$  and  $q_l^0$  ( $\Delta q_l = q_l^1 - q_l^0$ ) per time step. When  $\Delta q_l > 0$ , water vapor will be condensed. When  $\Delta q_l < 0$ , the excess liquid water will be

evaporated. Finally, temperature and water vapor tendency are updated correspondingly based on the liquid water tendency.

Because cloud fraction and condensate are derived from the same PDF, a consistency between them is automatically obtained and adjustment between cloud fraction and cloud water in the default Park-RH is no longer needed. The connection of subgrid-scale variance with the turbulence and shallow convection increases the flexibility of the approach to capture horizontal subgrid-scale variations. The impacts of the new approach on model simulations, especially on marine low clouds, will be described later.

### 3. Short-Term Hindcast and Evaluation

The VAMOS Ocean-Cloud-Atmosphere-Land Study Regional Experiment (VOCALS-REx) campaign was conducted during October and November 2008 to understand model simulation and predictability of the southeastern Pacific coupled atmosphere-ocean-land system (Wood et al., 2011). The main experiment was conducted within a domain ( $69^{\circ}\text{W}$ – $86^{\circ}\text{W}$ ,  $12^{\circ}\text{S}$ – $31^{\circ}\text{S}$ ) with most measurements concentrated along the  $20^{\circ}\text{S}$

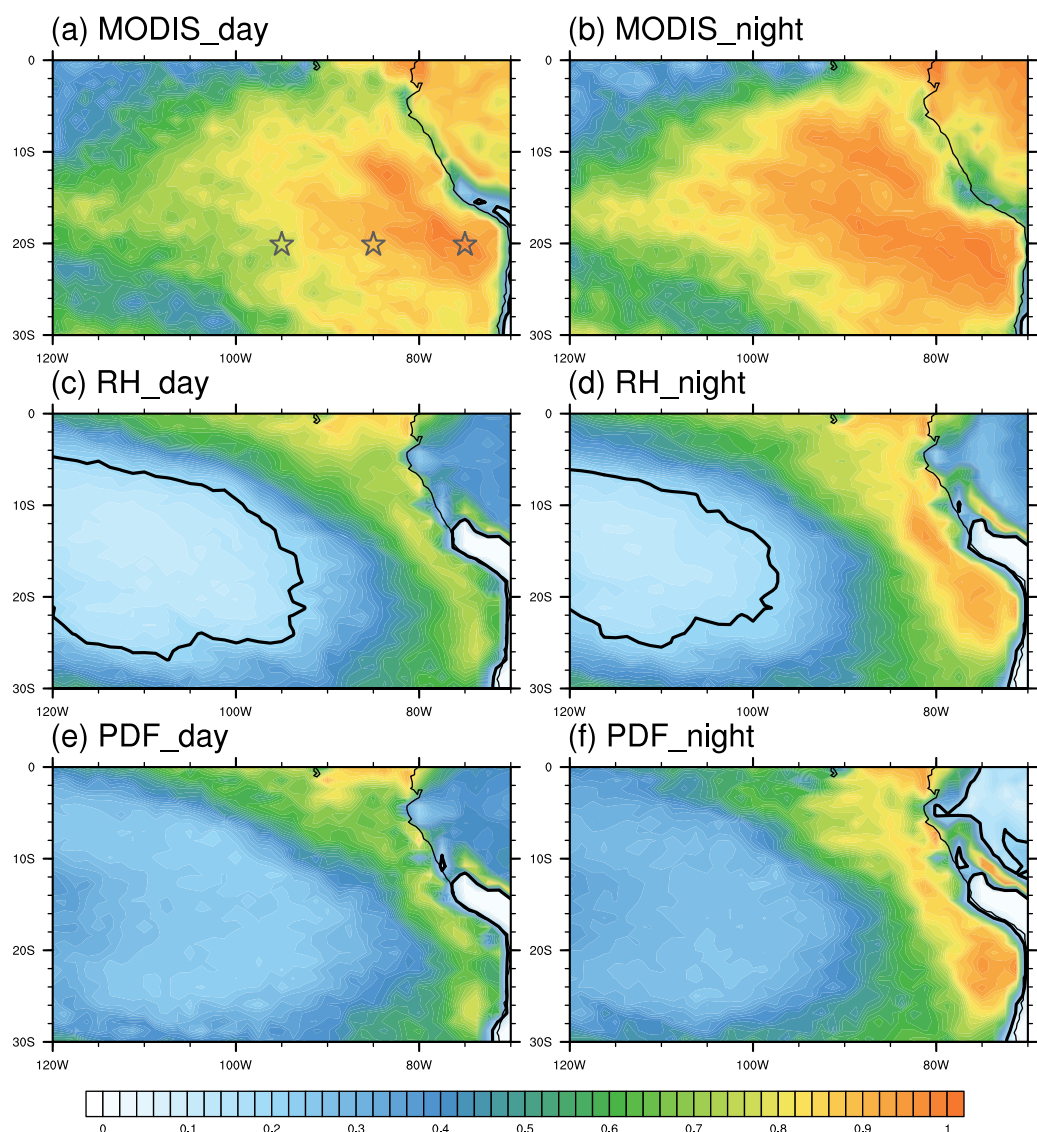


**Figure 2.** Mean low cloud fraction from (c, d) Park-RH and (e, f) Gauss-PDF compared with (a, b) total cloud fraction of MODIS Terra at (a, c, e) 10:30 LT and (b, d, f) 01:30 LT. The solid black lines indicate the contour of cloud fraction of 0.2. The stars indicate three sites: ( $20^{\circ}\text{S}$ ,  $75^{\circ}\text{W}$ ), ( $20^{\circ}\text{S}$ ,  $85^{\circ}\text{W}$ ), and ( $20^{\circ}\text{S}$ ,  $95^{\circ}\text{W}$ ).

latitude. High-resolution sounding profiles are interpolated to the model levels for easy comparisons. We focus on the boundary layer structure and diurnal variation of clouds at three sites ten degrees apart along the 20°S latitude (Figure 2) for detailed investigation.

In order to directly compare with observations, the short-term hindcast approach based on the Cloud-Associated Parameterizations Testbed (CAPT) is applied (Hannay et al., 2009; Ma et al., 2014; Phillips et al., 2004). Previous studies (Ma et al., 2014, 2015; Xie et al., 2012) indicated that the hindcast approach was able to capture model's systematic bias similar to that in the long-term climate simulations associated with fast physics. Compared with available observations, CAPT is a useful and efficient method to identify potential deficits in model parameterizations (Zheng et al., 2016). Model initializations, including the initial land states, follow Ma et al. (2015) and Zheng et al. (2016). Daily hindcasts were conducted and integrated for 5 days during the period from 15 October 2008 to 16 November 2008 using Park-RH and Gauss-PDF, respectively. In the Gauss-PDF simulation, we implemented the default RH-based cloud fraction scheme in it and then saved the cloud fraction from two cloud fraction schemes simultaneously. This ensures the same state variables are used for cloud fraction calculation from Gauss-PDF and Park-RH so that a direct comparison is possible. To reduce the sampling noise and better represent forecast errors, the third day forecasts from each 5 day simulation are averaged for the comparison with observations and detailed analysis. Note that the results do not change much with the choice of forecast day.

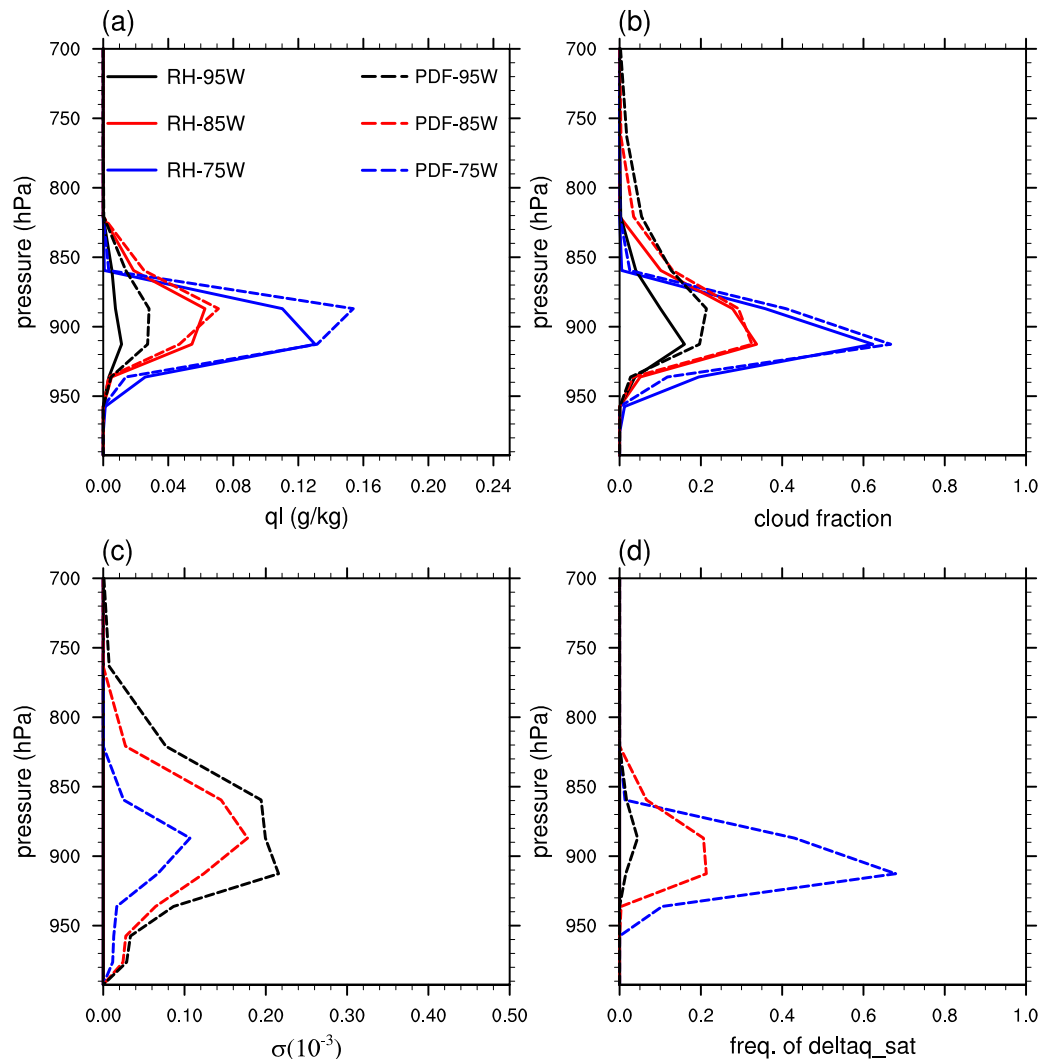


**Figure 3.** Vertical profile of (a) liquid water specific humidity, (b) cloud fraction, (c) subgrid-scale standard deviation, and (d) occurrence frequency of positive saturation deficit along the 20°S latitude at 75°W, 85°W, and 95°W from Park-RH and Gauss-PDF.

Horizontal distribution of low cloud fraction over southeastern Pacific Ocean is compared with that from the Moderate Resolution Imaging Spectrometer (MODIS) Terra satellite (data available at <https://giovanni.gsfc.nasa.gov/giovanni/>). Although MODIS measures the total cloud fraction rather than the low cloud fraction, low clouds dominate over this region and it is a reasonable comparison (e.g., Wyant et al., 2015). Figure 2 shows the low cloud fraction during daytime (10:30 LT) and nighttime (01:30 LT) from Park-RH and Gauss-PDF compared with MODIS. Marine low clouds are widespread over this vast area with cloud fractions up to 0.9 and larger than 0.5 over the whole area. There is a decrease of cloud fraction from the coast to the open ocean. In general, cloud fraction is 0.2 larger in the nighttime than in the daytime, especially over the open ocean. Overall, both Gauss-PDF and Park-RH are able to capture the spatial pattern of cloud distribution as MODIS, but they underestimate the cloud fraction over stratocumulus and trade cumulus regimes. The cloud fraction in the open ocean is below 0.2 during the daytime or nighttime in Park-RH (Figures 2c and 2d). Compared with Park-RH, Gauss-PDF increases the low cloud fraction almost over the whole region, and the most significant increase occurs over the open ocean region west of 90°W (Figures 2e and 2f). Previous studies found that the cloud fraction in CAM5 is too large near the coast, but decreases too sharply off the coast (Medeiros et al., 2012; Xiao et al., 2014). This sharp transition from stratocumulus to trade cumulus is alleviated in the new approach (Figures 2e and 2f), which is closer to observations (Figures 2a and 2b). Both simulations underestimate the contrast of cloud fraction between day and night though.

Figure 3 compares the cloud water, cloud fraction, subgrid-scale standard deviation, and occurrence frequency of positive saturation deficit at three sites (75°W, 85°W, and 95°W) along the 20°S latitude line. In general, both schemes capture the decreased cloud fraction and cloud water from 75°W to 95°W. This is due to the larger RH at 75°W in Park-RH, but due to the smaller subgrid-scale standard deviation (Figure 3c) and larger occurrence frequency of positive saturation deficit (Figure 3d) at 75°W in Gauss-PDF. As discussed in section 2, the larger occurrence frequency of positive saturation deficit and the smaller subgrid-scale variance lead to the larger cloud fraction. Compared with Park-RH, Gauss-PDF produces similar cloud fractions at 75°W and 85°W, but larger cloud fraction at 95°W (Figure 3b). Cloud water shares similar vertical profiles between the two schemes, but Gauss-PDF tends to produce more cloud water, especially at 95°W (Figure 3a). This is consistent with the better transition noted in Figure 2. Both Gauss-PDF and Park-RH are

also able to capture the diurnal change of cloud fraction and cloud water (not shown). For Park-RH, the diurnal change of clouds is mainly controlled by the diurnal change of RH induced by the boundary layer turbulence and occasionally active shallow convection. The diurnal variation of clouds in Gauss-PDF is mainly regulated by different subgrid-scale variances, which are closely connected with turbulent and shallow convective processes.

What contributes to the better transition in Gauss-PDF? More flexible and spatially varying subgrid-scale variances in Gauss-PDF enable such a smooth transition. The cloud fraction and subgrid-scale variance along a cross section at 20°S from 75°W to 120°W (Figure 4) well illustrate the transition from stratocumulus to trade cumulus. Note that the results here are from Gauss-PDF simulation in which cloud fractions from Park-RH and Gauss-PDF are derived from the same atmospheric state variables. The cloud fraction from Park-RH decreases sharply from 50% off the coast to 10% near 95°W, while Gauss-PDF produces larger cloud fraction over open ocean regions due to the larger subgrid-scale variance there. This is also consistent with the cloud fraction and cloud water profiles at the specific sites (Figure 3). For example, Gauss-PDF produces ~10% larger cloud fraction near 900 hPa at 90°W under the same RH situation (Figure 4). In Gauss-PDF, the increased subgrid-scale variance and the larger occurrence frequency of negative saturation deficit (Figure 3d) contribute to the increased cloud fraction westward. Since the critical RH in Park-RH only changes with height, it fails to capture the horizontal variation of subgrid-scale variance. This hinders the cloud formation over

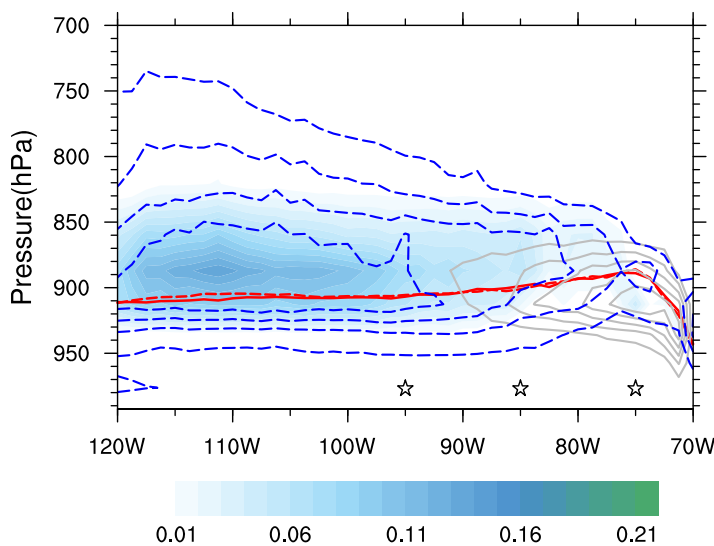


**Figure 4.** Longitude-vertical cross section of cloud fraction calculated from Park-RH (grey solid lines), subgrid-scale standard deviation from Gauss-PDF (blue dashed lines), the cloud fraction difference between Gauss-PDF and Park-RH (shaded), and the planetary boundary layer height (PBLH) from Park-RH (red solid line) and Gauss-PDF (red dashed line). The cloud fraction varies from 0.1 to 0.5 with an interval of 0.1. The subgrid-scale standard deviation varies from 0.05 to 0.2 with an interval of 0.05. Note that cloud fractions from Park-RH and Gauss-PDF are derived from the same thermodynamic variables (see text for more details).

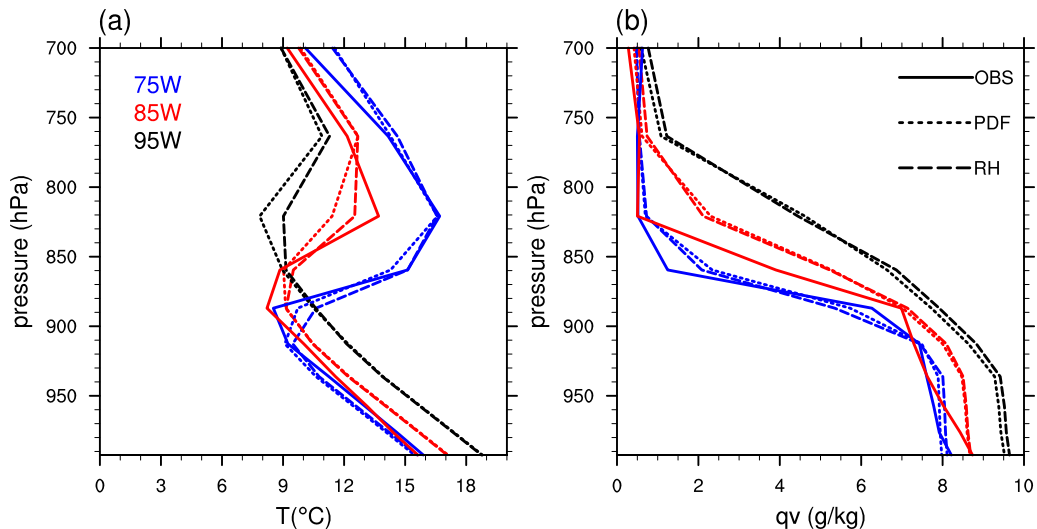


**Figure 5.** Vertical profiles of (a) temperature and (b) specific humidity from Park-RH (dashed), Gauss-PDF (dotted), and observation (solid) along the 20°S latitude at 75°W (blue), 85°W (red), and 95°W (black).

regions dominated by shallow convection because of the relatively low RH. Therefore, considering the subgrid-scale variance caused by turbulence and shallow convection in the new cloud scheme is the key to the improved cloud fraction. In addition, Gauss-PDF and Park-RH both share similar boundary layer height, which might be mainly controlled by the moist turbulence scheme (Bretherton & Park, 2009) instead of the cloud scheme.

Low clouds and boundary layer structure are closely linked with each other. It is illuminating to see how boundary layer structure changes with improved cloud fraction and cloud water (Figure 5). Limited by available observed data set, we only show the corresponding observations at 75°W and 85°W. Overall, both simulations are able to capture the basic structure of observed boundary layer with a few notable differences. First, Park-RH and Gauss-PDF both have warm and moist biases in the lower levels, especially at 85°W, as also noted in Hannay et al. (2009) and Medeiros et al. (2012). The planetary boundary layer (PBL) is shallower and over well mixed in two simulations over the open oceans compared with observations. Second, the influence of Gauss-PDF is mainly concentrated within and above the cloud layer.

Compared with Park-RH, the overall warmer cloud layer in Gauss-PDF is due to the larger cloud water in the new cloud scheme (Figure 3a). Over the open ocean region, larger condensation induces more latent heat release, which results in a warmer cloud layer than that in Park-RH. The exaggerated warm bias in Gauss-PDF above the cloud layer (Figure 5a) mainly comes from the stronger turbulent transport and large-scale subsidence via preliminary temperature budget analysis (not shown). There is no significant change of water vapor specific humidity in two simulations (Figure 5b). Overall, by changing condensation and further interacting with other processes, Gauss-PDF has the ability to modify the boundary layer structure. The sub-cloud layer structure, which is mainly regulated by the boundary layer scheme, is influenced negligibly by the new cloud scheme.

#### 4. Long-Term Simulation and Evaluation

Long-term simulations were conducted at the horizontal resolution of 0.9° latitude × 1.25° longitude with 30 vertical levels. Six year Atmospheric Model Intercomparison Project (AMIP)-type simulations forced by observed climatological SST and sea ice were performed with Park-RH and Gauss-PDF scheme, respectively. The last 5 year monthly outputs are used for the following analysis. Note that the Coupled Model Intercomparison Project (CMIP) Observation Satellite Package (COSP; Kay et al., 2012) is turned on to better compare with satellite observations.

To evaluate the model performance, simulation results are compared with available observation data sets. Observations include global total precipitation from GPCP (Global Precipitation Climatology Project;

**Table 1**  
Global Mean Climatological Properties of Park-RH, Gauss-PDF, and Observations

Property	Park-RH	Gauss-PDF	OBS
Low cloud amount (%)	42.78	41.56	43.01 <sup>a</sup>
Middle cloud amount (%)	24.96	24.60	32.16 <sup>a</sup>
High cloud amount (%)	37.89	36.91	40.33 <sup>a</sup>
Total cloud amount (%)	63.73	63.29	66.82 <sup>a</sup>
TOA net long wave flux ( $\text{W m}^{-2}$ )	236.81	238.14	239.67 <sup>b</sup>
TOA net short wave flux ( $\text{W m}^{-2}$ )	236.09	236.27	239.67 <sup>b</sup>
TOA imbalance ( $\text{W m}^{-2}$ )	-0.72	-1.87	0.81
Shortwave cloud forcing ( $\text{W m}^{-2}$ )	-54.24	-54.26	-47.15 <sup>b</sup>
Longwave cloud forcing ( $\text{W m}^{-2}$ )	22.66	21.12	26.06 <sup>b</sup>
Precipitation rate ( $\text{mm d}^{-1}$ )	3.05	3.03	2.67 <sup>c</sup>
Liquid water path ( $\text{g m}^{-2}$ )	52.18	74.50	78.94 <sup>d</sup>

<sup>a</sup>CloudSat. <sup>b</sup>CERES-EBAF. <sup>c</sup>GPCP. <sup>d</sup>NVAP.

Huffman et al., 2009), low cloud fraction from ISCCP-D2 data set (International Satellite Cloud Climatology Project [July 1983 to December 2001]; Rossow & Schiffer, 1991), cloud fraction from CloudSat (Stephens et al., 2002), liquid water path (LWP) over the ocean from NVAP (NASA Water Vapor Project [January 1998 to December 1999]; Randel et al., 1996), top of atmosphere (TOA) longwave and shortwave flux including shortwave cloud forcing (SWCF) and longwave cloud forcing (LWCF) from the CERES-EBAF (Clouds and the Earth's Radiation Energy Systems Energy Balanced and Filled; Loeb et al., 2009). The vertical distribution of cloud fraction is from CALIPSO GOCCP data set (The GCM-Oriented CALIPSO Cloud Product [June 2006 to December 2010]; Chepfer et al., 2010).

Mean climate from the two simulations compared with available observations is summarized in Table 1. The TOA imbalance is slightly decreased to  $-1.87 \text{ W m}^{-2}$  in Gauss-PDF from  $-0.7 \text{ W m}^{-2}$  in Park-RH. However, such a small TOA imbalance can be obviated by slightly increasing the precipitation efficiency in the large-scale or convective precipitation processes. Note that cloud improvements discussed later (section 4.2) do not change much with the magnitude of the TOA imbalance (not shown). Furthermore, a TOA radiation balance can be achieved in the short-coupled simulation as discussed in section 4.5.

#### 4.1. Cloud and Radiation

Low clouds are prevalent over eastern tropical and subtropical ocean and midlatitude storm track regions (Figure 6), and their formation is associated with the subsiding branch of Hadley Cell and midlatitude storm activities (Klein & Hartmann, 1993; Wood, 2012). Compared with the observation, Park-RH is able to capture the spatial pattern of low cloud distribution. One prominent discrepancy between Park-RH and observations is a significant underestimate (15–25%) of low cloud fraction over the subtropical open ocean regions, and

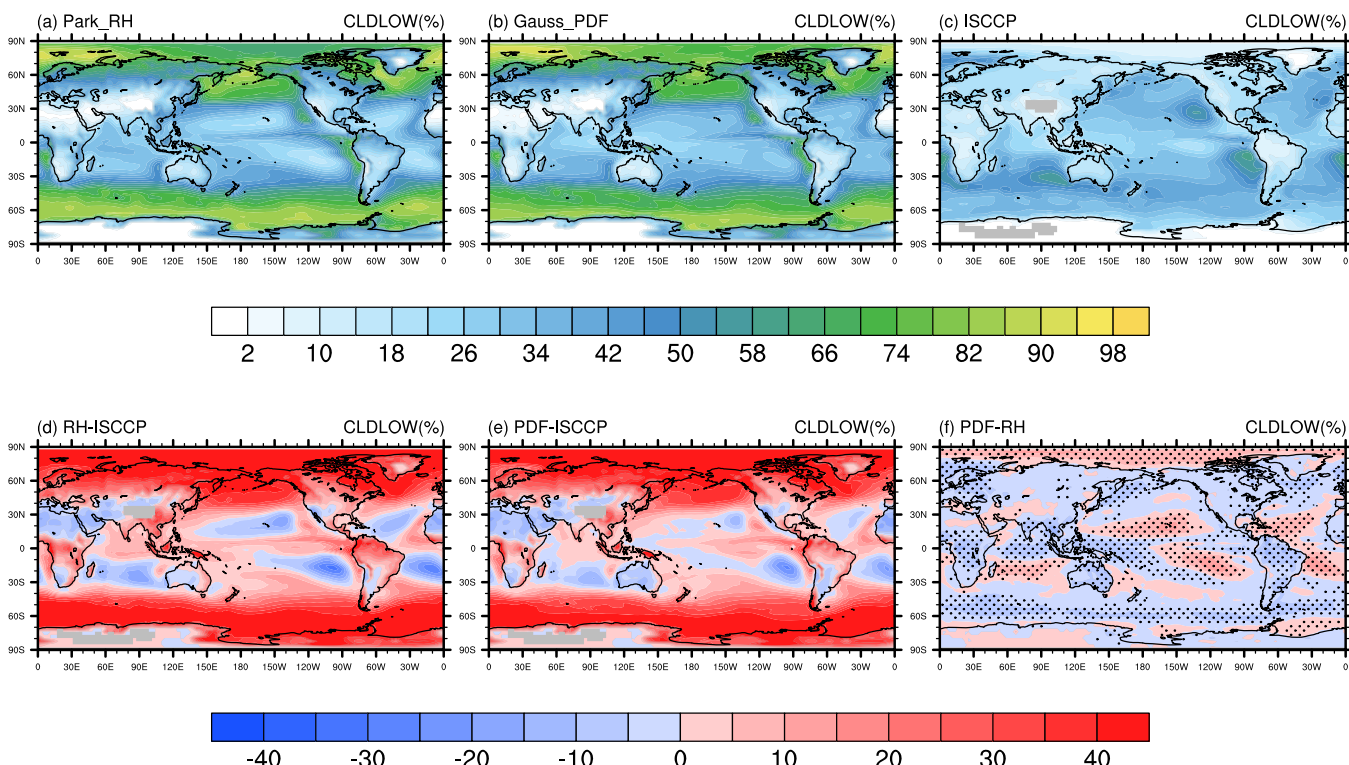


**Figure 6.** Annual mean low cloud fraction (%) from (a) Park-RH, (b) Gauss-PDF, (c) ISCCP, and the difference between (d) Park-RH and ISCCP, (e) Gauss-PDF and ISCCP, and (f) Gauss-PDF and Park-RH. The stippled areas indicate that the difference between Gauss-PDF and Park-RH is statistically significant at 0.05 level.

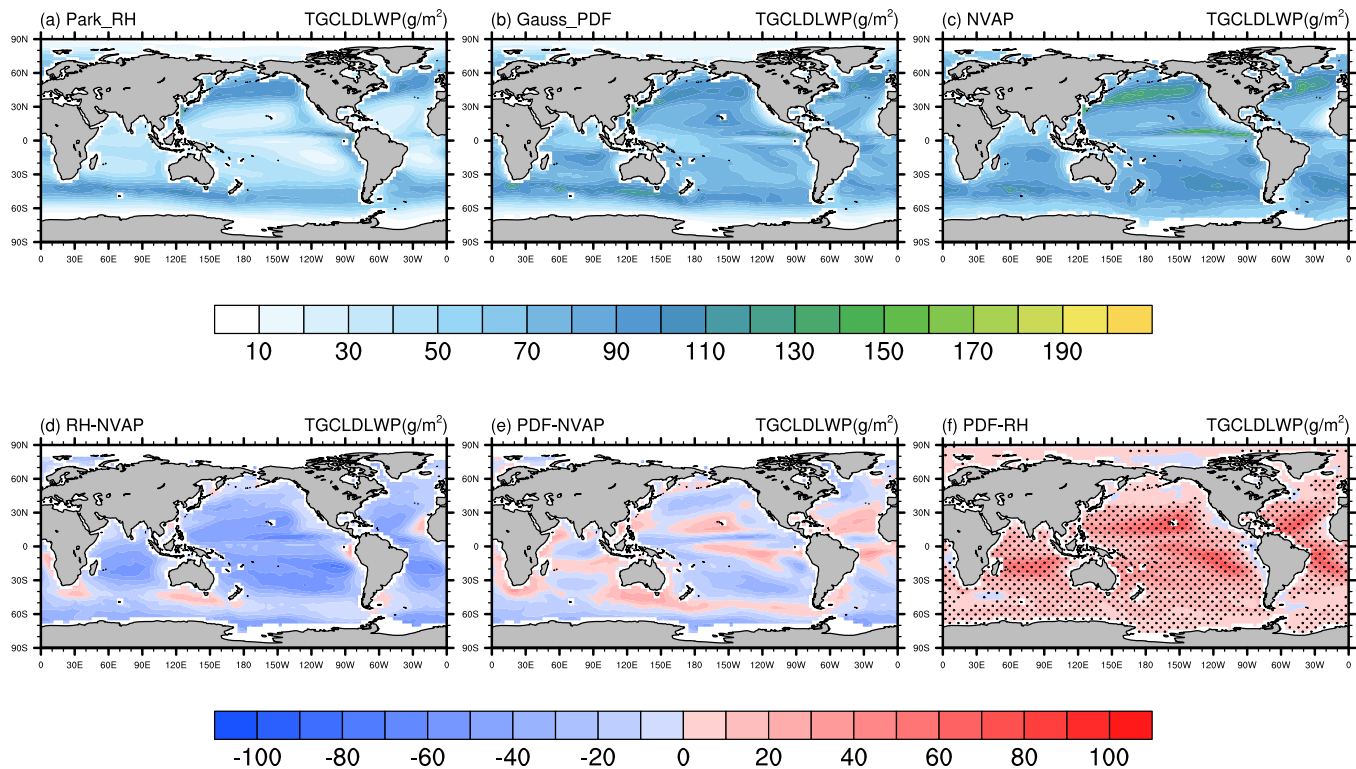


**Figure 7.** Annual mean liquid water path ( $\text{g m}^{-2}$ ) over the ocean from (a) Park-RH, (b) Gauss-PDF, and (c) NVAP and the difference between (d) Park-RH and NVAP, (e) Gauss-PDF and NVAP, and (f) Gauss-PDF and Park-RH. The stippled areas indicate that the difference between Gauss-PDF and Park-RH is statistically significant at 0.05 level.

an overestimate of  $\sim 20\%$  near the subtropical coastal regions (Figure 6d). In contrast, Gauss-PDF is able to reduce these biases over these regions, especially over the subtropical open ocean regions (Figure 6f). For example, Gauss-PDF increases the low cloud fraction by  $\sim 15\%$  over the trade cumulus region in the southeastern Pacific Ocean. In the midlatitude storm track regions, Gauss-PDF also mitigates the bias slightly. Improvements of low cloud simulation over the subtropical ocean regions in Gauss-PDF (Figure 6f) are directly related to the inclusion of subgrid-scale variance from turbulent and shallow convective processes. Low clouds over deep convective regions are slightly reduced by 5–10%, probably due to the exclusion of effects from deep convection. As a result, there is a slight decrease of global mean low cloud fraction from 42.78% to 41.56% (Table 1) despite the increased low clouds over subtropical ocean regions.

Similar to low cloud fraction, the annual mean LWP is also improved in Gauss-PDF (Figure 7). The global mean LWP over the ocean increases from  $52.18 \text{ g m}^{-2}$  in Park-RH to  $74.50 \text{ g m}^{-2}$  in Gauss-PDF, closer to  $78.94 \text{ g m}^{-2}$  of NVAP (Table 1). Compared with the observation, both schemes underestimate LWP over ocean regions, especially in the deep convection and subtropical ocean regions; however, they both show reasonable spatial patterns. Different from low cloud fraction, LWP is increased over all ocean regions in Gauss-PDF compared with Park-RH. The largest increase in Gauss-PDF is around  $70 \text{ g m}^{-2}$  over the subtropical eastern ocean regions (Figure 7f). Analysis indicates that the increased LWP is mainly related to the increased condensation rate caused by the subgrid-scale variance in Gauss-PDF. The increase of LWP over trade wind regions is kind of exaggerated in Gauss-PDF (Figure 7e), which is directly related to the large subgrid-scale variance (Figure 8a). Some studies indicate that the precipitation term is also a dominant budget term in the subgrid-scale variance equations in precipitating shallow cumulus clouds and the precipitation could decrease the variances at cloudy altitudes (Griffin & Larson, 2016; Schemann & Seifert, 2017). Therefore, neglecting the precipitation term could lead to overestimated variance in regions dominated by precipitating shallow convection, which may cause the overestimated LWP near the equator in Gauss-PDF. Modifications by including the impact of precipitation on subgrid-scale variance and relating subgrid-scale variance to the autoconversion in the large-scale stratiform clouds will be reported in a future study.

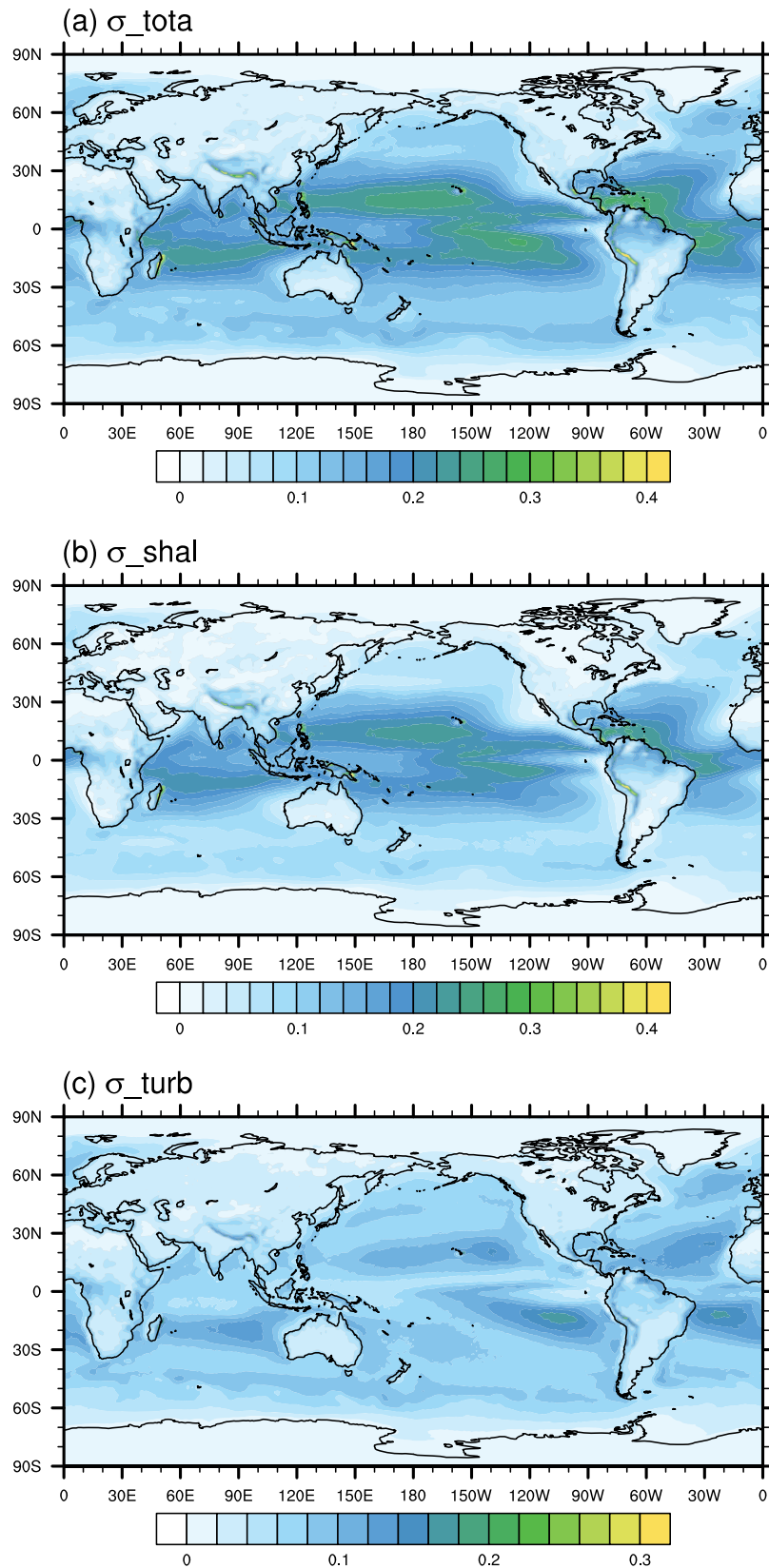


**Figure 8.** The annual subgrid-scale standard deviations from Gauss-PDF caused by (a) turbulence and shallow convection, (b) only shallow convection, and (c) only turbulence at 912 hPa.

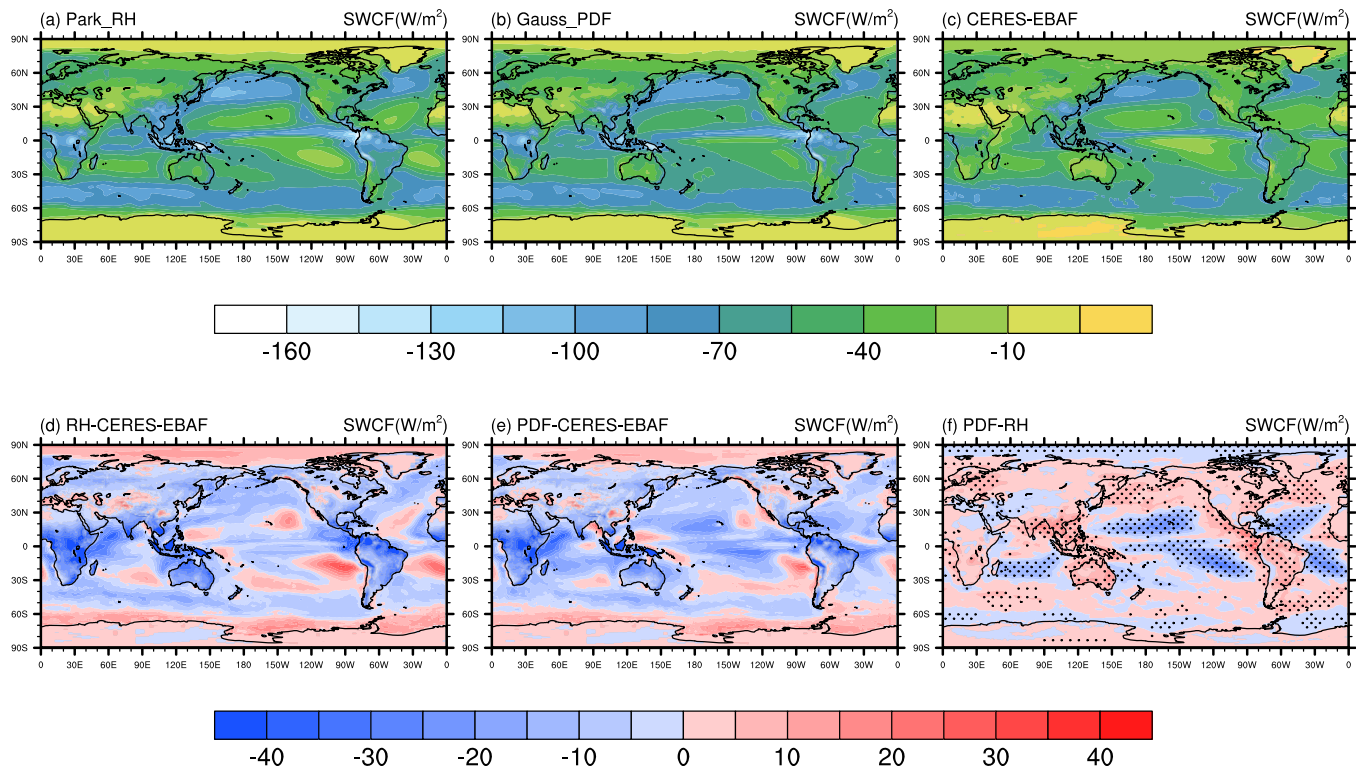


**Figure 9.** Annual mean shortwave cloud forcing ( $\text{W m}^{-2}$ ) from (a) Park-RH, (b) Gauss-PDF, and (c) CERES-EBAF, and the difference between (d) Park-RH and CERES-EBAF, (e) Gauss-PDF and CERES-EBAF, and (f) Gauss-PDF and Park-RH. The stippled areas indicate that the difference between Gauss-PDF and Park-RH is statistically significant at 0.05 level.

As mentioned in section 2, cloud fraction and cloud water in Gauss-PDF are directly related to the subgrid-scale variance. Figure 8 shows the annual mean total subgrid-scale variance and those related to turbulent and shallow convective processes, respectively near 900 hPa. We choose 900 hPa as the reference level because low cloud fraction and cloud water maximize near this level (Figure 3). Overall, variances from shallow convection and turbulence play different roles in different regions. The total variance is dominated by the variance from shallow convection over the open ocean. The largest subgrid-scale variance is located over the subtropical trade wind regions, resulting from the inclusion of the variance from the shallow convection. Obviously, the spatial pattern of subgrid-scale variance from Gauss-PDF dominates the cloud fraction and LWP differences between Gauss-PDF and Park-RH.

With improved low cloud fraction and LWP, SWCF also changes in Gauss-PDF. The global mean SWCF is  $-54.24 \text{ W m}^{-2}$  in Park-RH and  $-54.26 \text{ W m}^{-2}$  in Gauss-PDF (Table 1). Park-RH overestimates the magnitude of SWCF over most regions, except for the subtropical ocean and polar regions (Figure 9d). The overestimated cloud fraction (Figure 6d) likely contributes to the overestimated magnitude of SWCF over most tropical land regions. Over the subtropical ocean regions, underestimated magnitude of SWCF varying from 20 to  $40 \text{ W m}^{-2}$  is attributed to the underestimated low cloud fraction (Figure 6d) and LWP (Figure 7d) in Park-RH. These biases are mitigated considerably in Gauss-PDF. The bias over the tropical land regions is reduced by about 50%. The most prominent improvement occurs in the southeastern Pacific Ocean, where the bias is alleviated by 50% due to the increased low cloud fraction and LWP (Figures 6f and 7f). Note that SWCF over the tropical middle Pacific Ocean is exaggerated (Figure 9e), which is likely due to the overestimated cloud fraction (Figure 6e) and LWP (Figure 7e). Overall, the better low cloud and LWP distribution contribute to the improved SWCF over the eastern subtropical open ocean regions.

#### 4.2. Vertical Cloud Structure

Three representative cross sections of low clouds off the coast of North America (California:  $20^{\circ}\text{N}$ – $30^{\circ}\text{N}$ ,  $120^{\circ}\text{W}$ – $160^{\circ}\text{W}$ ), South America (Peru:  $10^{\circ}\text{S}$ – $20^{\circ}\text{S}$ ,  $80^{\circ}\text{W}$ – $120^{\circ}\text{W}$ ) and South Africa (Namibia:  $10^{\circ}\text{S}$ – $20^{\circ}\text{S}$ ,  $0^{\circ}\text{W}$ – $30^{\circ}\text{W}$ ) are compared among the two schemes with CALIPSO GOCCP data set (June 2006 to December 2010;

Chepfer et al., 2010) as a reference (Figure 10). Cloud fraction decreases, but cloud top height and cloud thickness increase away from the shore in observations. Off the Peruvian coastal region, the cloud fraction in Park-RH has a maximum value around 50% near the coast, but sharply declines from 40% to below 20% near 90°W, and then remains at 15% westward. Gauss-PDF well captures this transition with cloud fraction maintained at 25% even near 100°W. Furthermore, cloud fraction is still above 20% near 850 hPa even further westward. Obviously, this is in better agreement with the observation (Figure 10c). Increased cloud fraction is also detected over Californian and Namibian regions. In addition, Gauss-PDF is able to capture the observed elevated cloud top height off the coast to some extent. Since Gauss-PDF focuses on the

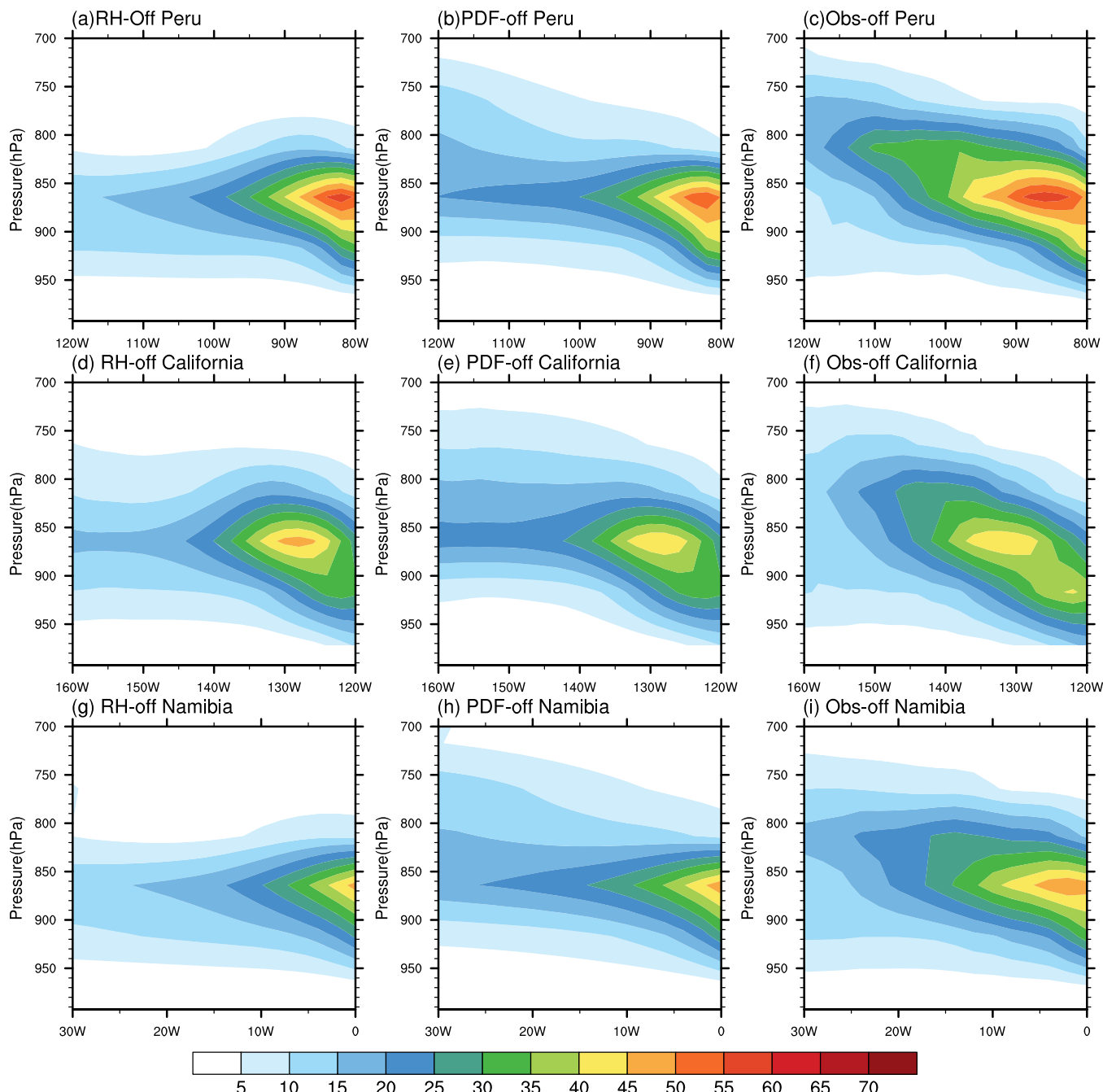


**Figure 10.** Vertical cross sections of annual mean cloud fraction (%) for (left) Park-RH, (middle) Gauss-PDF, and (right) CALIPSO observation averaged over (a–c) 10°S–20°S (west of South America), (d–f) 20°S–30°S (west of North America), and (g–i) 10°S–20°S (west of South Africa).

subgrid-scale variance from other processes, the increased cloud fraction offshore corresponds to the spatial distribution of subgrid-scale variance like that shown in the CAPT simulations (Figure 4).

A simulation using the Gauss-PDF scheme, but only including the subgrid-scale variance from turbulence scheme, is unable to capture the significant increase of clouds further off the coast (not shown). Including the effect of shallow convection on the subgrid-scale variance leads to the better performance because the shallow convection is active over the open ocean region and contribute significantly to the total variance as shown in Figure 8. In this sense, inclusion of subgrid-scale variance from shallow convection is critical for improved low cloud simulations, especially over the trade cumulus regions.

#### 4.3. Impacts on the Mean Climate

Compared with Park-RH, the global mean precipitation rate reduces from  $3.05 \text{ mm d}^{-1}$  to  $3.03 \text{ mm d}^{-1}$  in Gauss-PDF (Table 1). The reduction is significant in the tropics where convective precipitation is dominant, especially over the tropical Pacific Ocean and equatorial western Indian Ocean (Figure 11). Partitioning between convective and large-scale precipitation further suggests that the difference of total precipitation between Gauss-PDF and Park-RH is mainly due to changes of convective precipitation (Figure 12f). The large-scale precipitation increases over the whole tropics (Figure 12c), but they are mostly smaller than  $0.5 \text{ mm d}^{-1}$ . There is also a slight increase of precipitation over the Maritime Continent and Indian continents (Figure 11f), and both convective and large-scale precipitation play a role in this. Overall, these changes to some extent mitigate the double intertropical convergence zone (ITCZ) problem in most GCMs (Lin, 2007) by a reduction of precipitation over ITCZ and an increase of precipitation near the equator. Why the modification of cloud scheme leads to the change of precipitation amount, distribution and partitioning between convective and large-scale precipitation warrants further studies.

Although Gauss-PDF increased low cloud fraction over subtropical ocean regions, it decreased low clouds in the deep tropics (Figure 6f) and thus resulted in a smaller global mean low cloud fraction (Table 1). This has been discussed in section 4.1. The global mean high clouds slightly reduced by  $\sim 1\%$ . Overall, total cloud

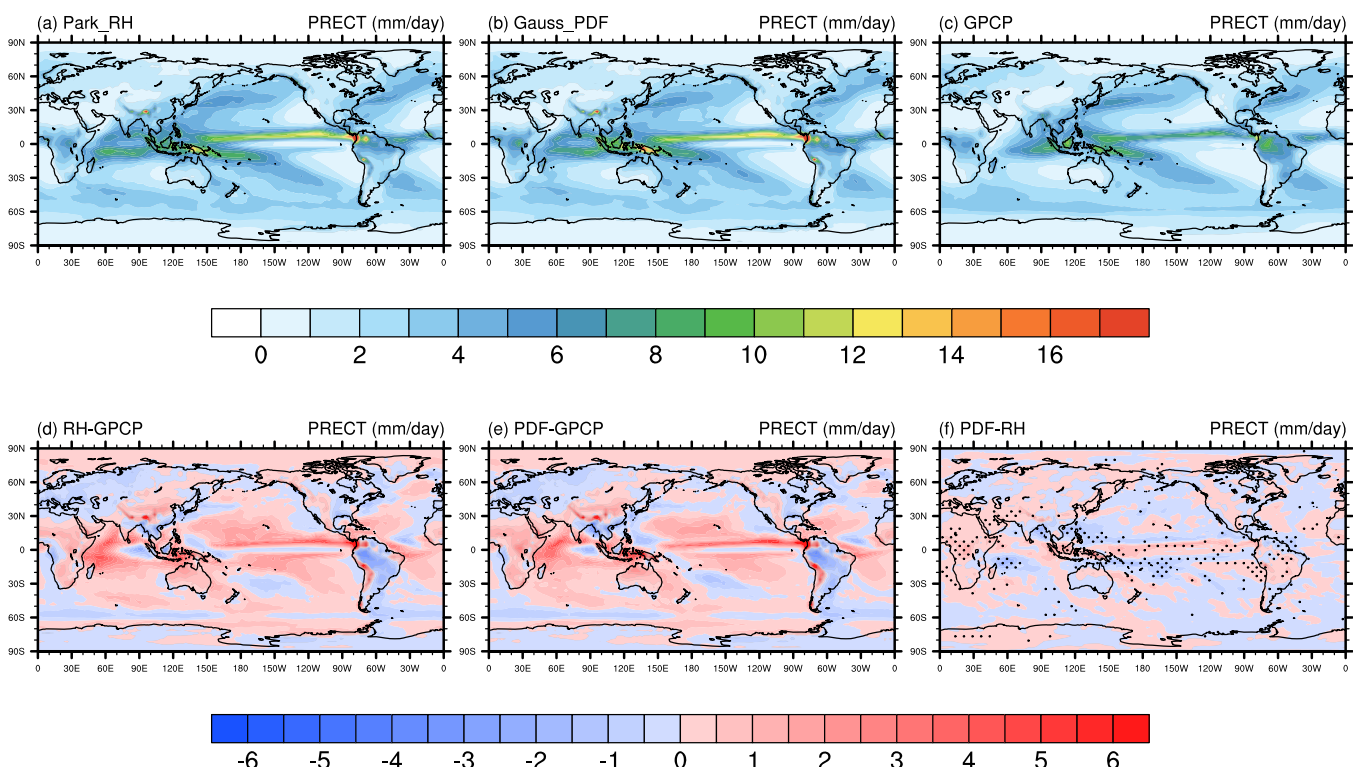


**Figure 11.** Annual mean total precipitation rate (mm/d) from (a) Park-RH, (b) Gauss-PDF, (c) GPCP, and the difference between (d) Park-RH and GPCP, (e) Gauss-PDF and GPCP, and (f) Gauss-PDF and Park-RH. The stippled areas indicate that the difference between Gauss-PDF and Park-RH is statistically significant at 0.05 level.

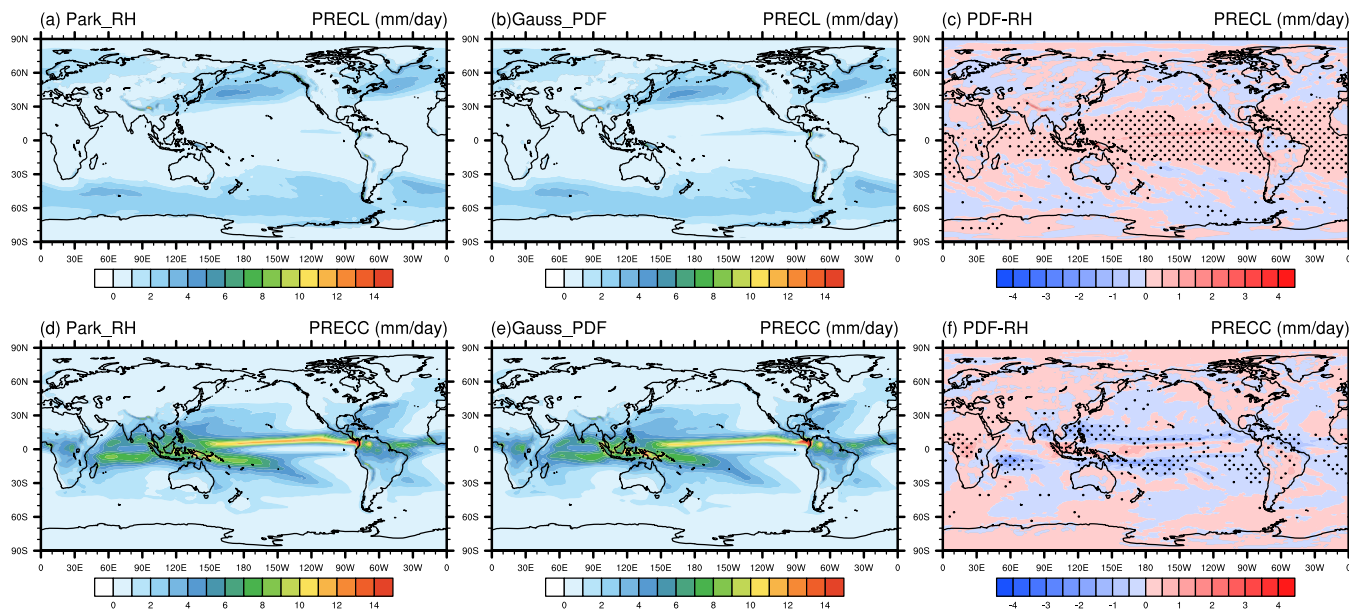


**Figure 12.** (a–c) Annual mean large-scale precipitation rate and (e–f) convective precipitation rate (mm/d) from (a, d) Park-RH, (b, e) Gauss-PDF, and (c, f) the difference between Gauss-PDF and Park-RH. The stippled areas indicate that the difference between Gauss-PDF and Park-RH is statistically significant at 0.05 level.

fraction was decreased from 63.73% in Park-RH to 63.29% in Gauss-PDF. Underestimate of high clouds likely contributes to the underestimated LWCF in two schemes. Compared with Park-RH, Gauss-PDF slightly underestimates LWCF by about  $1.5 \text{ W m}^{-2}$ , which is likely attributed to the reduced high clouds and decreased cloud top height.

A Taylor diagram (Figure 13) shows the overall performance of the simulations against observations in terms of the correlation and normalized standard deviation (Taylor, 2001). A better model performance is closer to the reference point. Compared with Park-RH, Gauss-PDF reduces the normalized standard deviation for most variables except for surface pressure and total precipitation, but correlation is degraded slightly for most variables except for the low cloud fraction.

SWCF is significantly improved with the normalized standard deviation decreased from 1.160 to 1.092. The correlation of low cloud fraction is slightly increased from 0.740 in Park-RH to 0.743 in Gauss-PDF. The reduced normalized standard deviations for most variables suggest that the new cloud scheme is able to improve some facets of the model, especially low cloud fraction and cloud forcing.

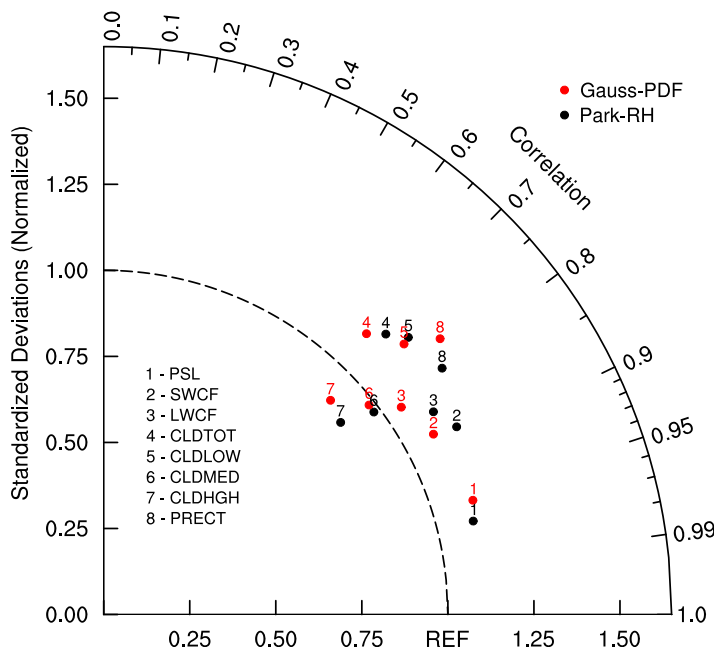


**Figure 13.** Taylor diagram for annual-mean sea level pressure (SLP), short wave cloud forcing (SWCF), longwave cloud forcing (LWCF), total cloud fraction (CLDTOT), low cloud fraction (CLDLOW), middle cloud fraction (CLDMED), high cloud fraction (CLDHGH), and total precipitation (PRECT) for Park-RH (black dots) and Gauss-PDF (red dots).

#### 4.4. Sensitivity to Horizontal Resolutions

Previous studies indicate that simulations of marine boundary layer clouds are sensitive to model resolutions (Kuwano-Yoshida et al., 2010; McCaa & Bretherton, 2004). Although Gauss-PDF performs well with  $1^\circ$  horizontal resolution, whether it is sensitive to different model resolutions is unknown. Another  $2^\circ$  AMIP simulation using the identical configurations as those of  $1^\circ$  simulation was conducted.

Overall, Gauss-PDF produces similar mean climate in the  $2^\circ$  simulation with slightly reduced TOA net SW flux, TOA net LW flux, and precipitation (Table 2). Improved low clouds and SWCF were maintained in the  $2^\circ$  simulation, and the difference of low clouds between the two simulations is smaller than 4% over most regions (Figure 14b). The  $1^\circ$  simulation has more low clouds over coastal regions (California, Peru, and Namibia) probably due to better resolved topography. But the increase of low clouds north of the equator in the eastern Pacific

**Table 2**  
Global Mean Climatological Properties of Various Runs

Resolution Simulation type	Gauss-PDF		Gauss-PDF	Park-RH
	0.9° × 1.25°	1.9° × 2.5°	1.9° × 2.5°	1.9° × 2.5°
	AMIP	AMIP	Coupled	Coupled
Low cloud amount (%)	41.56	42.94	39.00	43.23
Total cloud amount (%)	63.29	64.49	59.77	63.86
Precipitation rate ( $\text{mm d}^{-1}$ )	3.03	2.96	3.01	3.01
TOA net LW flux ( $\text{W m}^{-2}$ )	238.14	235.40	240.79	236.11
TOA net SW flux ( $\text{W m}^{-2}$ )	236.27	234.19	240.85	236.28
TOA imbalance ( $\text{W m}^{-2}$ )	-1.87	-1.21	0.06	0.17

fixed forcings in 1850 for 12 years are conducted using Park-RH and Gauss-PDF, respectively. First, both Park-RH and Gauss-PDF produce reasonable net TOA radiative fluxes with the TOA radiation balance obtained after a few years of spin-up. The TOA imbalance is  $0.06 \text{ W m}^{-2}$  for Gauss-PDF and  $0.17 \text{ W m}^{-2}$  for Park-RH (Table 2). Second, improvement of low clouds still remains in the coupled simulation (Figure 15). Gauss-PDF increases low clouds over the subtropical eastern ocean, especially the trade wind regions, which is similar to that in the AMIP simulation (Figure 6f). At the same time, global mean low clouds and total clouds slightly decrease after the air sea interaction, which increases the global mean TOA radiative fluxes accordingly (Table 2).

As mentioned in section 4.3, Gauss-PDF has the ability to alleviate the double ITCZ problem to some extent. Figure 16 gives the seasonal evolution of total precipitation rate from GPCP, Park-RH, and Gauss-PDF over

Ocean (Figure 14b) warrants further investigation. Low clouds decrease with increased resolution over most land regions (Figure 14b). Another significant decrease is over the southeastern Pacific Ocean dominated by stratocumulus and stratocumulus-to-cumulus transition. The sensitivity of SWCF to resolution is basically identical to that of low clouds (Figure 14d). The comparison suggests that Gauss-PDF is not very sensitive to horizontal resolution and the improvement can be achieved at various resolutions.

#### 4.5. Preliminary Results From the Coupled Simulations

TOA radiation balance is a prerequisite for the coupled simulations. In addition, whether the improvement of low clouds still presents in the coupled simulation is unknown. Two degree coupled simulations with

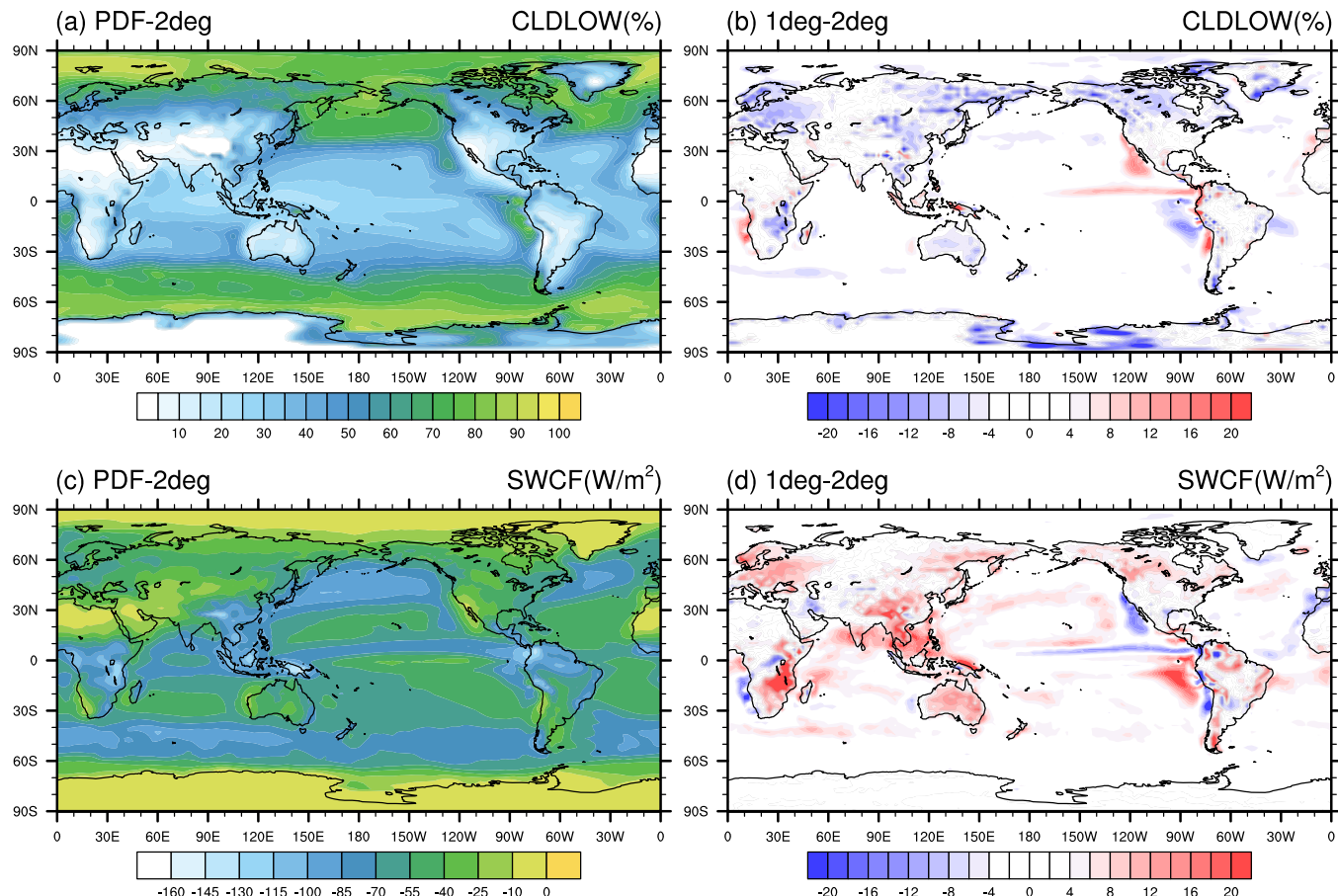


**Figure 14.** (a, b) Annual mean low cloud fraction (%) and (c, d) SWCF ( $\text{W m}^{-2}$ ) from the  $2^\circ$  simulation with (a, c) Gauss-PDF and (b, d) the difference relative to the  $1^\circ$  Gauss-PDF simulation shown in Figure 6b.

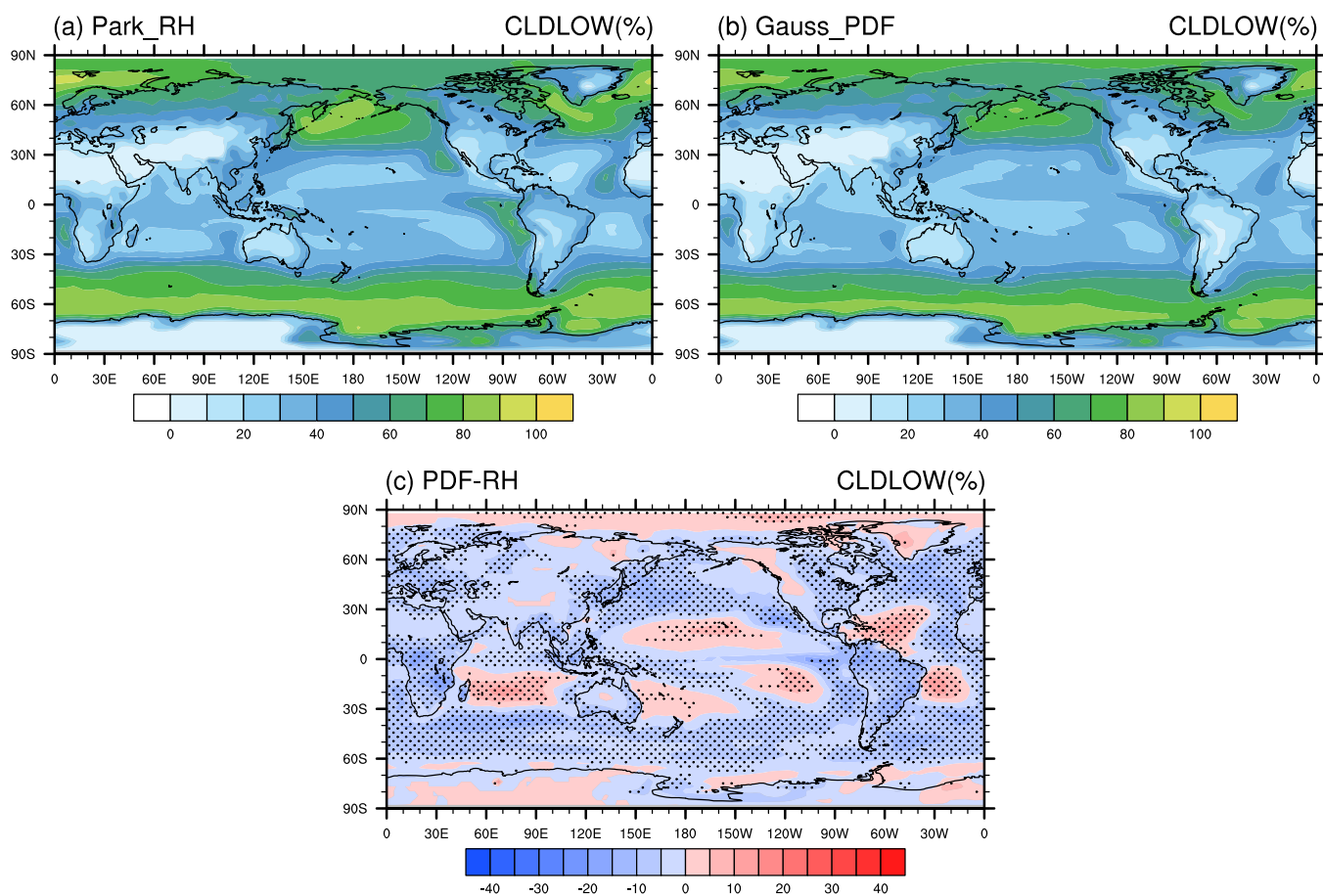


**Figure 15.** Annual mean low cloud fraction (%) from (a) Park-RH, (b) Gauss-PDF, and (c) the difference between Gauss-PDF and Park-RH in coupled simulations. The stippled areas indicate that the difference between Gauss-PDF and Park-RH is statistically significant at 0.05 level.

eastern Pacific ( $180^{\circ}\text{E}$ – $90^{\circ}\text{W}$ ) in the coupled simulations. ITCZ is mostly located north of the equator throughout the whole year except for a weak peak during the boreal spring in GPCP (Figure 16a). In contrast, Park-RH produces too much precipitation south of the equator all year round (Figure 16d) with

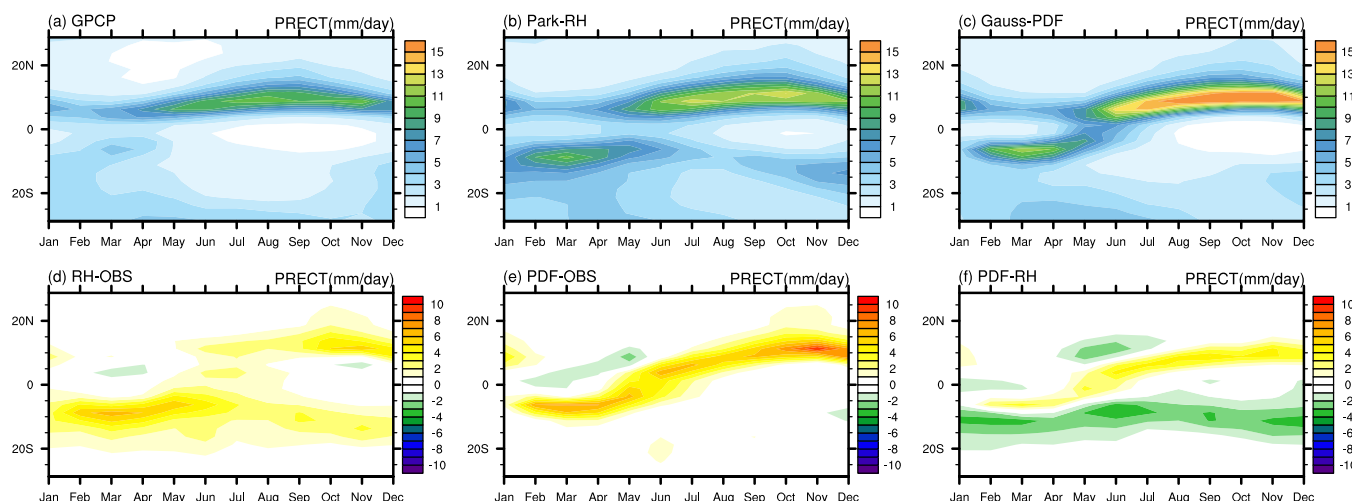


**Figure 16.** Seasonal evolution of 11 year (years 2–12) mean total precipitation rates (mm/d) over eastern Pacific ( $180^{\circ}\text{E}$ – $90^{\circ}\text{W}$ ) from (a) GPCP, (b) Park-RH, (c) Gauss-PDF, and the difference between (d) Park-RH and GPCP, (e) Gauss-PDF and GPCP, and (f) Gauss-PDF and Park-RH.

overestimated precipitation over the equator. Instead, the seasonal cycle of precipitation from Gauss-PDF is closer to GPCP, especially regarding the reduction of excessive precipitation south of the equator from boreal summer to fall (Figure 16f). However, precipitation is still overestimated in both Park-RH and Gauss-PDF. The causes for the alleviated double ITCZ problem will be studied in the future.

## 5. Discussion and Conclusions

Continued efforts have been given to improve the low cloud simulation in GCMs. In this study, we propose a simple diagnostic statistical cloud scheme aiming to improve low cloud simulations. Assuming a Gaussian PDF distribution for the combined variable of liquid water potential temperature and total specific humidity, its variance is parameterized by including the effect of turbulent and shallow convective processes on the subgrid-scale variability. The close connection between cloud scheme and related physical processes in Gauss-PDF is crucial to the improvement of subtropical low clouds. Meanwhile, the new scheme diagnoses the cloud fraction and cloud condensate from the same PDF, so the consistency between cloud fraction and cloud condensate is obtained automatically. The “empty” or “dense” clouds will not appear in this scheme, and the adjustment between cloud water and cloud fraction in the default RH scheme is no longer needed.

The approach is implemented and tested in CAM5. CAPT simulations indicated that the approach generates more cloud fraction and cloud water over the southeastern Pacific Ocean region and agrees better with observations from the VOCALS-REx campaign. Gauss-PDF produces greater cloud fraction than Park-RH over the open ocean region given the same thermodynamic states. This suggests that the improved cloud simulation is mainly due to the inclusion of the subgrid-scale variance from shallow convection and turbulence, rather than different basic states. At the same time, the new cloud scheme is able to produce relatively realistic boundary layer structures, especially over the open ocean region, although the weaker inversion strength still persists.

Long-term global simulation using the new cloud scheme gives an overall slightly better mean climate than that using the default scheme. Gauss-PDF captures the basic climatological structure of low clouds and LWP. Compared with Park-RH, Gauss-PDF reduces the negative bias of low clouds over the subtropical eastern ocean regions, making the transition from stratocumulus-to-cumulus clouds smoother. Increased low clouds accompanied by increased LWP contribute to an improved TOA radiation and an alleviation of SWCF bias over the subtropical regions. This improvement results from the consideration of subgrid-scale variances from turbulent and shallow convective processes, which increases the direct connection between cloud formation and related physical processes. Simulations at different horizontal resolutions indicate that the approach is not sensitive to resolutions. Preliminary coupled simulations suggest that TOA radiation balance can be rather easily obtained with similar performance of low clouds compared to atmospheric only simulations. The alleviated double ITCZ problem using the new scheme indicates that cloud simulation can impact tropical precipitation and circulation significantly.

Compared to the relative simple approach introduced here, a more complex scheme named as Cloud Layers Unified by Binormals (CLUBB) has been implemented and tested in CAM5 (Bogenschutz et al., 2012, 2013). Because CLUBB combines shallow convection, turbulence, and cloud macrophysics in the same scheme, it avoids the potential inconsistencies introduced by separately representing different physical processes using different parameterizations. In addition, higher-order turbulence closure directly predicts the subgrid-scale variability of vertical velocity, which is critical for aerosol activation. However, much reduced time steps lead to significantly increased computational cost using CLUBB. Meanwhile, the complexity of the scheme makes the understanding and tuning of the scheme not as straightforward as Gauss-PDF.

Both CLUBB and Gauss-PDF avoid the inconsistency between cloud fraction and cloud water, and thus the adjustment between them is no longer needed. One of the advantages of both schemes is the improved trade cumulus and stratocumulus-to-cumulus transition although the reasons might differ. Clouds over the coastal regions are reduced in Gauss-PDF, but they are increased in CLUBB (Bogenschutz et al., 2013). LWP changes also differ between the two approaches. CLUBB prognoses shallow convection and turbulence in a unified framework and its calculation of subgrid-scale variances contains budgets (Griffin & Larson, 2016) for processes such as advection, turbulent (gradient) production, turbulent dissipation, and precipitation.

This allows users to distinguish the contribution of each physical process. Gauss-PDF diagnoses the subgrid-scale variance from shallow convection and turbulence separately and thus is computationally more efficient due to its simplicity. In both approaches, it is advantageous to be able to distinguish the contributions of physical processes. In terms of the complexity, the two approaches go to two extremes, and an intermediate complexity approach might be more appropriate.

As we discussed above, although Gauss-PDF with parameterized subgrid-scale variance from turbulence and shallow convection is proved to be effective in alleviating low cloud bias, more explorations are needed. First, this research mainly focuses on low cloud simulations, so the effect from deep convection has not been included. Hence, a potential inconsistency between stratiform clouds and deep convection clouds might still exist. A more self-consistent and unified approach to handle all types of clouds is necessary in the future. Second, considering the higher-order moments, like skewness, might be necessary under the complex situation when multiple cloud types coexist. Third, the effect of precipitation of shallow convection on the subgrid-scale variance needs to be considered. Finally, improvement of cloud simulation is an integral process requiring interactions among various physical processes.

## Appendix A: Derivation of Subgrid-Scale Variance From Turbulence and Shallow Convection

The covariance tendency equation of two variables  $A$  and  $B$  with neglected advection terms is expressed as

$$\frac{\partial \overline{A'B'}}{\partial t} = -\frac{\partial \overline{w'A'B'}}{\partial z} - \left[ \overline{w'A'} \frac{\partial B}{\partial z} + \overline{w'B'} \frac{\partial A}{\partial z} \right] - \epsilon_{AB} \quad (\text{A1})$$

where  $A'B'$  can represent any combination of  $\theta_l$  and/or  $q_w$ . The three terms in the right-hand side are the turbulent transport, gradient production, and molecular dissipation term, respectively. Considering the relative importance of each term in the cloud layer to produce the partial cloudiness, the transport term can be neglected. Therefore, assuming steady state, one can get a balance between gradient production term and molecular dissipation term:

$$-\left[ \overline{w'A'} \frac{\partial B}{\partial z} + \overline{w'B'} \frac{\partial A}{\partial z} \right] - \epsilon_{AB} = 0 \quad (\text{A2})$$

Referring to the moist turbulence scheme (Bretherton & Park, 2009) in CAM5 and using the notions there, the dissipation term can be expressed as

$$\begin{aligned} \epsilon_{ab} &= \frac{\overline{A'B'}}{\tau} \\ &= \frac{\overline{A'B'}}{l_k/\sqrt{e}} \end{aligned} \quad (\text{A3})$$

where  $\tau$  is the dissipation time scale,  $e$  is the turbulent kinetic energy, and  $l_k$  is the dissipation length scale, which is written as  $l_k = c_{AB}l$ , with  $l$  the master turbulent length scale and  $c_{AB}$  a constant.

Turbulent fluxes are written as

$$\begin{aligned} \overline{w'A'} &= -K_h \frac{\partial A}{\partial z} \\ &= -IS_h \sqrt{e} \frac{\partial A}{\partial z} \end{aligned} \quad (\text{A4})$$

with  $S_h$  being the nondimensional stability function.

Combining equations (A2)–(A4) with some algebra, we finally get

$$\overline{A'B'} = 2S_h c_{AB} l^2 \frac{\partial A}{\partial z} \frac{\partial B}{\partial z} \quad (\text{A5})$$

Therefore, the variance of  $s$  ( $\sigma_s^2$ ) from turbulence is expressed as

$$\begin{aligned}\sigma_{st}^2 &= \frac{1}{4} \left( a^2 \overline{q'_w{}^2} + b^2 \overline{\theta'_l{}^2} - 2ab \overline{q'_w \theta'_l} \right) \\ &= c_1 S_h l^2 \left( a^2 \left( \frac{\partial q_w}{\partial z} \right)^2 + b^2 \left( \frac{\partial \theta_l}{\partial z} \right)^2 - 2ab \frac{\partial q_w}{\partial z} \frac{\partial \theta_l}{\partial z} \right)\end{aligned}\quad (\text{A6})$$

here  $c_1 = c_{AB}/2 = 3.57$  according to the closure of moist turbulence scheme. However, considering the uncertainty of the dissipation turbulence scale (Bretherton & Park, 2009, equation (3)), we recommend  $c_1$  as a tuning parameter in a range of 1.0–8.0.

Similarly, the balance equation (A2) is also used to derive the subgrid-scale variance from shallow convection. The main difference is the parameterization of dissipation term and turbulent flux term, which are based on the mass flux in shallow convection scheme.

The dissipation term is expressed as

$$\begin{aligned}\epsilon_{ab,scu} &= \frac{\overline{A'B'}}{\tau_{scu}} \\ &= \frac{\overline{A'B'}}{I_{clu}/w^*}\end{aligned}\quad (\text{A7})$$

where  $I_{clu}$  is the cloud depth of shallow convection and  $w^*$  is the convective velocity scale from the turbulence scheme.

The turbulent flux term is written as

$$\overline{w'A'} = M_{scu} (\bar{A}_u - \bar{A}) \quad (\text{A8})$$

where  $M_{scu}$  is the mass flux of shallow convection, with the unit of m/s.

Thus, we can get the expression of  $A'B'$  from shallow convection:

$$\overline{q'_w{}^2} = -2M_{scu} (q_{w,u} - \bar{q}_w) \frac{\partial \bar{q}_w}{\partial z} \frac{I_{clu}}{w^*} \quad (\text{A9})$$

$$\overline{\theta'_l{}^2} = -2M_{scu} (\theta_{l,u} - \bar{\theta}_l) \frac{\partial \bar{\theta}_l}{\partial z} \frac{I_{clu}}{w^*} \quad (\text{A10})$$

$$\overline{q'_w \theta'_l} = - \left( M_{scu} (q_{w,u} - \bar{q}_w) \frac{\partial \bar{\theta}_l}{\partial z} + M_{scu} (\theta_{l,u} - \bar{\theta}_l) \frac{\partial \bar{q}_w}{\partial z} \right) \frac{I_{clu}}{w^*} \quad (\text{A11})$$

Therefore, the subgrid-scale variance from shallow convection is

$$\begin{aligned}\sigma_{ss}^2 &= \frac{1}{4} \left( a^2 \overline{q'_w{}^2} + b^2 \overline{\theta'_l{}^2} - 2ab \overline{q'_w \theta'_l} \right) = -\frac{1}{2} M_{scu} \frac{I_{clu}}{w^*} * \\ &\quad \left\{ a^2 (q_{w,u} - \bar{q}_w) \frac{\partial \bar{q}_w}{\partial z} + b^2 (\theta_{l,u} - \bar{\theta}_l) \frac{\partial \bar{\theta}_l}{\partial z} - ab \left[ (\theta_{l,u} - \bar{\theta}_l) \frac{\partial \bar{q}_w}{\partial z} + (q_{w,u} - \bar{q}_w) \frac{\partial \bar{\theta}_l}{\partial z} \right] \right\}\end{aligned}\quad (\text{A12})$$

## References

- Ahlgrimm, M., & Forbes, R. (2014). Improving the representation of low clouds and drizzle in the ECMWF model based on ARM observations from the Azores. *Monthly Weather Review*, 142(2), 668–685. <https://doi.org/10.1175/MWR-D-13-00153.1>
- Bechtold, P., Pinty, J. P., & Fraval, C. (1992). A model of marine boundary-layer cloudiness for mesoscale applications. *Journal of the Atmospheric Sciences*, 49(18), 1723–1744. [https://doi.org/10.1175/1520-0469\(1992\)049<1723:AMOMBL>2.0.CO;2](https://doi.org/10.1175/1520-0469(1992)049<1723:AMOMBL>2.0.CO;2)
- Bogenschutz, P. A., Gettelman, A., Morrison, H., Larson, V. E., Craig, C., & Schanen, D. P. (2013). Higher-order turbulence closure and its impact on climate simulations in the Community Atmosphere Model. *Journal of Climate*, 26(23), 9655–9676. <https://doi.org/10.1175/JCLI-D-13-00075.1>
- Bogenschutz, P. A., Gettelman, A., Morrison, H., Larson, V. E., Schanen, D. P., Meyer, N. R., et al. (2012). Unified parameterization of the planetary boundary layer and shallow convection with a higher-order turbulence closure in the Community Atmosphere Model: Single-column experiments. *Geoscientific Model Development*, 5(6), 1407–1423. <https://doi.org/10.5194/gmd-5-1407-2012>
- Bony, S., & Dufresne, J.-L. (2005). Marine boundary layer clouds at the heart of tropical cloud feedback uncertainties in climate models. *Geophysical Research Letters*, 32, L20806. <https://doi.org/10.1029/2005GL023851>
- Bony, S., & Emanuel, K. A. (2001). A parameterization of the cloudiness associated with cumulus convection; evaluation using TOGA COARE data. *Journal of the Atmospheric Sciences*, 58(21), 3158–3183. [https://doi.org/10.1175/1520-0469\(2001\)058<3158:APOTCA>2.0.CO;2](https://doi.org/10.1175/1520-0469(2001)058<3158:APOTCA>2.0.CO;2)

## Acknowledgments

We are grateful for constructive comments and suggestions from Peter Caldwell and two anonymous reviewers. This work was supported by the National Natural Science Foundation of China (41775098) and the outreach project of the State Key Laboratory of Severe Weather, Chinese Academy of Meteorological Sciences (2016LASW-B02). HM and SX were funded by the Regional and Global Climate Modeling, Atmospheric System Research, and Atmospheric Radiation Measurement Programs of the U.S. DOE, and their work was performed under the auspices of the U.S. DOE by Lawrence Livermore National Laboratory under contract DE-AC52-07NA27344. We gratefully acknowledge the groups of ERA-Interim (<https://www.ecmwf.int/en/research/climate-reanalysis/era-interim>), CALIPSO-GOCCP (<http://climserv.ipsl.polytechnique.fr/cfmip-obs/>), CERES-EBAF (<https://ceres.larc.nasa.gov/products.php?product=EBAF-TOA>), ISCCP (<https://isccp.giss.nasa.gov/products/onlineData.html>), NVAP ([https://eosweb.larc.nasa.gov/project/nvap/nvap\\_ng\\_lwp\\_table](https://eosweb.larc.nasa.gov/project/nvap/nvap_ng_lwp_table)), GPCP (<https://www.esrl.noaa.gov/psd/data/gridded/data.gpcp.html>), CloudSat (<http://cloudsat.atmos.colostate.edu>), and VOCALS-Rex ([http://data.eol.ucar.edu/master\\_list/?project=VOCALS](http://data.eol.ucar.edu/master_list/?project=VOCALS)) for providing public access to various observational data sets. The forcing data for the CAPT simulations are provided by the U.S. Department of Energy, Cloud-Associated Parameterizations Testbed (CAPT) group at Lawrence Livermore National Laboratory. The source code of the scheme is available at <https://github.com/yanluan-thu/pdf-cloud>.

- Bony, S., Stevens, B., Frierson, D. M., Jakob, C., Kageyama, M., Pincus, R., et al. (2015). Clouds, circulation and climate sensitivity. *Nature Geoscience*, 8(4), 261–268. <https://doi.org/10.1038/ngeo2398>
- Bougeault, P. (1981). Modeling the trade-wind cumulus boundary layer. Part I: Testing the ensemble cloud relations against numerical data. *Journal of the Atmospheric Sciences*, 38(11), 2414–2428. [https://doi.org/10.1175/1520-0469\(1981\)038<2414:MTTWC>2.0.CO;2](https://doi.org/10.1175/1520-0469(1981)038<2414:MTTWC>2.0.CO;2)
- Bougeault, P. (1982). Cloud-ensemble relations based on the gamma probability distribution for the higher-order models of the planetary boundary layer. *Journal of the Atmospheric Sciences*, 39(12), 2691–2700. [https://doi.org/10.1175/1520-0469\(1982\)039<2691:CERBOT>2.0.CO;2](https://doi.org/10.1175/1520-0469(1982)039<2691:CERBOT>2.0.CO;2)
- Bretherton, C. S., & Park, S. (2009). A new moist turbulence parameterization in the Community Atmosphere Model. *Journal of Climate*, 22(12), 3422–3448. <https://doi.org/10.1175/2008JCLI2556.1>
- Cheng, A., & Xu, K.-M. (2015). Improved low-cloud simulation from the Community Atmosphere Model with an advanced third-order turbulence closure. *Journal of Climate*, 28(14), 5737–5762. <https://doi.org/10.1175/JCLI-D-14-00776.1>
- Chepfer, H., Bony, S., Winker, D., Cesana, G., Dufresne, J. L., Minnis, P., et al. (2010). The GCM-oriented CALIPSO cloud product (CALIPSO-GOCCP). *Journal of Geophysical Research*, 115, D00H16. <https://doi.org/10.1029/2009JD012251>
- Donner, L. J., Wyman, B. L., Hemler, R. S., Horowitz, L. W., Ming, Y., Zhao, M., et al. (2011). The dynamical core, physical parameterizations, and basic simulation characteristics of the atmospheric component AM3 of the GFDL global coupled model CM3. *Journal of Climate*, 24(13), 3484–3519. <https://doi.org/10.1175/2011JCLI3955.1>
- Golaz, J.-C., Larson, V. E., & Cotton, W. R. (2002). A PDF-based model for boundary layer clouds. Part I: Method and model description. *Journal of the Atmospheric Sciences*, 59(24), 3540–3551. [https://doi.org/10.1175/1520-0469\(2002\)059<3540:APBMFB>2.0.CO;2](https://doi.org/10.1175/1520-0469(2002)059<3540:APBMFB>2.0.CO;2)
- Gregory, D., Wilson, D., & Bushell, A. (2002). Insights into cloud parametrization provided by a prognostic approach. *Quarterly Journal of the Royal Meteorological Society*, 128(583), 1485–1504. <https://doi.org/10.1002/qj.200212858305>
- Griffin, B. M., & Larson, V. E. (2016). Parameterizing microphysical effects on variances and covariances of moisture and heat content using a multivariate probability density function: A study with CLUBB (tag MVCS). *Geoscientific Model Development*, 9(11), 4273–4295. <https://doi.org/10.5194/gmd-9-4273-2016>
- Guo, H., Golaz, J.-C., Donner, L. J., Ginoux, P., & Hemler, R. S. (2014). Multivariate probability density functions with dynamics in the GFDL atmospheric general circulation model: Global tests. *Journal of Climate*, 27(5), 2087–2108. <https://doi.org/10.1175/JCLI-D-13-00347.1>
- Hannay, C., Williamson, D. L., Hack, J. J., Kiehl, J. T., Olson, J. G., Klein, S. A., et al. (2009). Evaluation of forecasted southeast pacific stratocumulus in the NCAR, GFDL, and ECMWF models. *Journal of Climate*, 22(11), 2871–2889. <https://doi.org/10.1175/2008JCLI2479.1>
- Hartmann, D. L. (1994). *Global physical climatology*. San Diego, CA, Academic Press.
- Hourdin, F., Mauritsen, T., Gettelman, A., Golaz, J.-C., Balaji, V., Duan, Q., et al. (2017). The art and science of climate model tuning. *Bulletin of the American Meteorological Society*, 98(3), 589–602. <https://doi.org/10.1175/BAMS-D-15-00135.1>
- Huffman, G. J., Adler, R. F., Bolvin, D. T., & Gu, G. (2009). Improving the global precipitation record: GPCP version 2.1. *Geophysical Research Letters*, 36, L17808. <https://doi.org/10.1029/2009GL040000>
- Kay, J. E., Hillman, B. R., Klein, S. A., Zhang, Y., Medeiros, B., Pincus, R., et al. (2012). Exposing global cloud biases in the Community Atmosphere Model (CAM) using satellite observations and their corresponding instrument simulators. *Journal of Climate*, 25(15), 5190–5207. <https://doi.org/10.1175/JCLI-D-11-00469.1>
- Kay, J. E., Wall, C., Yettella, V., Medeiros, B., Hannay, C., Caldwell, P., et al. (2016). Global climate impacts of fixing the Southern Ocean shortwave radiation bias in the Community Earth System Model (CESM). *Journal of Climate*, 29(12), 4617–4636. <https://doi.org/10.1175/JCLI-D-15-0358.1>
- Klein, S. A., & Hartmann, D. L. (1993). The seasonal cycle of low stratiform clouds. *Journal of Climate*, 6(8), 1587–1606. [https://doi.org/10.1175/1520-0442\(1993\)006<1587:TSCOLS>2.0.CO;2](https://doi.org/10.1175/1520-0442(1993)006<1587:TSCOLS>2.0.CO;2)
- Kuwano-Yoshida, A., Enomoto, T., & Ohfuchi, W. (2010). An improved PDF cloud scheme for climate simulations. *Quarterly Journal of the Royal Meteorological Society*, 136(651), 1583–1597. <https://doi.org/10.1002/qj.660>
- Lewellen, W. S., & Yoh, S. (1993). Binormal model of ensemble partial cloudiness. *Journal of the Atmospheric Sciences*, 50(9), 1228–1237. [https://doi.org/10.1175/1520-0469\(1993\)050<1228:BMOEPC>2.0.CO;2](https://doi.org/10.1175/1520-0469(1993)050<1228:BMOEPC>2.0.CO;2)
- Lin, J.-L. (2007). The Double-ITCZ problem in IPCC AR4 coupled GCMs: Ocean–atmosphere feedback analysis. *Journal of Climate*, 20(18), 4497–4525. <https://doi.org/10.1175/JCLI4272.1>
- Lin, Y. (2014). Humidity variability revealed by a sounding array and its implications for cloud representation in GCMs. *Journal of Geophysical Research: Atmospheres*, 119, 10499–10514. <https://doi.org/10.1002/2014JD021837>
- Lin, Y., Donner, L. J., Petch, J., Bechtold, P., Boyle, J., Klein, S. A., et al. (2012). TWP-ICE global atmospheric model intercomparison: Convective responsiveness and resolution impact. *Journal of Geophysical Research*, 117, D09111. <https://doi.org/10.1029/2011JD017018>
- Lock, A. P., Brown, A. R., Bush, M. R., Martin, G. M., & Smith, R. N. B. (2000). A new boundary layer mixing scheme. Part I: Scheme description and single-column model tests. *Monthly Weather Review*, 128(9), 3187–3199. [https://doi.org/10.1175/1520-0493\(2000\)128<3187:ANBLMS>2.0.CO;2](https://doi.org/10.1175/1520-0493(2000)128<3187:ANBLMS>2.0.CO;2)
- Loeb, N. G., Wielicki, B. A., Doelling, D. R., Smith, G. L., Keyes, D. F., Kato, S., et al. (2009). Toward optimal closure of the earth's top-of-atmosphere radiation budget. *Journal of Climate*, 22(3), 748–766. <https://doi.org/10.1175/2008JCLI2637.1>
- Luhar, A. K., Hibberd, M. F., & Hurley, P. J. (1996). Comparison of closure schemes used to specify the velocity pdf in Lagrangian stochastic dispersion models for convective conditions. *Atmospheric Environment*, 30(9), 1407–1418. [https://doi.org/10.1016/1352-2310\(95\)00464-5](https://doi.org/10.1016/1352-2310(95)00464-5)
- Ma, H.-Y., Chuang, C. C., Klein, S. A., Lo, M.-H., Zhang, Y., Xie, S., et al. (2015). An improved hindcast approach for evaluation and diagnosis of physical processes in global climate models. *Journal of Advances in Modeling Earth Systems*, 7, 1810–1827. <https://doi.org/10.1002/2015MS000490>
- Ma, H.-Y., Xie, S., Klein, S. A., Williams, K. D., Boyle, J. S., Bony, S., et al. (2014). On the correspondence between mean forecast errors and climate errors in CMIP5 models. *Journal of Climate*, 27(4), 1781–1798. <https://doi.org/10.1175/JCLI-D-13-00474.1>
- Mauritsen, T., Stevens, B., Roeckner, E., Crueger, T., Esch, M., Giorgi, M., et al. (2012). Tuning the climate of a global model. *Journal of Advances in Modeling Earth Systems*, 4, M00A01. <https://doi.org/10.1029/2012MS000154>
- McCaa, J. R., & Bretherton, C. S. (2004). A new parameterization for shallow cumulus convection and its application to marine subtropical cloud-topped boundary layers. Part II: Regional simulations of marine boundary layer clouds. *Monthly Weather Review*, 132(4), 883–896. [https://doi.org/10.1175/1520-0493\(2004\)132<0883:ANPFSC>2.0.CO;2](https://doi.org/10.1175/1520-0493(2004)132<0883:ANPFSC>2.0.CO;2)
- Medeiros, B., Williamson, D. L., Hannay, C., & Olson, J. G. (2012). Southeast pacific stratocumulus in the Community Atmosphere Model. *Journal of Climate*, 25(18), 6175–6192. <https://doi.org/10.1175/JCLI-D-11-00503.1>
- Mellor, G. L. (1977). The Gaussian cloud model relations. *Journal of the Atmospheric Sciences*, 34(2), 356–358. [https://doi.org/10.1175/1520-0469\(1977\)034<0356:TGCMR>2.0.CO;2](https://doi.org/10.1175/1520-0469(1977)034<0356:TGCMR>2.0.CO;2)

- Naumann, A. K., Seifert, A., & Mellado, J. P. (2013). A refined statistical cloud closure using double-Gaussian probability density functions. *Geoscientific Model Development*, 6(5), 1641–1657. <https://doi.org/10.5194/gmd-6-1641-2013>
- Neale, R. B., Chen, C., Lauritzen, P. H., Williamson, D. L., Conley, A. J., Smith, A. K., et al. (2012). *Description of the NCAR Community Atmosphere Model (CAM 5.0)* (NCAR Tech. Note NCAR/TN-4861 STR). Boulder, CO: National Center for Atmospheric Research. Retrieved from [http://www.cesm.ucar.edu/models/cesm1.0/cam/docs/description/cam5\\_desc.pdf](http://www.cesm.ucar.edu/models/cesm1.0/cam/docs/description/cam5_desc.pdf)
- Park, S., & Bretherton, C. S. (2009). The University of Washington shallow convection and moist turbulence schemes and their impact on climate simulations with the Community Atmosphere Model. *Journal of Climate*, 22(12), 3449–3469. <https://doi.org/10.1175/2008JCLI2557.1>
- Park, S., Bretherton, C. S., & Rasch, P. J. (2014). Integrating cloud processes in the Community Atmosphere Model. version 5. *Journal of Climate*, 27(18), 6821–6856. <https://doi.org/10.1175/JCLI-D-14-00087.1>
- Phillips, T. J., Potter, G. L., Williamson, D. L., Cederwall, R. T., Boyle, J. S., Fiorino, M., et al. (2004). Evaluating parameterizations in general circulation models: Climate simulation meets weather prediction. *Bulletin of the American Meteorological Society*, 85(12), 1903–1915. <https://doi.org/10.1175/BAMS-85-12-1903>
- Quaas, J. (2012). Evaluating the critical relative humidity as a measure of subgrid-scale variability of humidity in general circulation model cloud cover parameterizations using satellite data. *Journal of Geophysical Research*, 117, D09208. <https://doi.org/10.1029/2012JD017495>
- Randel, D. L., Greenwald, T. J., Haar, T. H. V., Stephens, G. L., Ringerud, M. A., & Combs, C. L. (1996). A new global water vapor dataset. *Bulletin of the American Meteorological Society*, 77(6), 1233–1246. [https://doi.org/10.1175/1520-0477\(1996\)077<1233:ANGWVD>2.0.CO;2](https://doi.org/10.1175/1520-0477(1996)077<1233:ANGWVD>2.0.CO;2)
- Rossov, W. B., & Schiffer, R. A. (1991). ISCCP cloud data products. *Bulletin of the American Meteorological Society*, 72(1), 2–20. [https://doi.org/10.1175/1520-0477\(1991\)072<0002:ICDP>2.0.CO;2](https://doi.org/10.1175/1520-0477(1991)072<0002:ICDP>2.0.CO;2)
- Schemann, V., & Seifert, A. (2017). A budget analysis of the variances of temperature and moisture in precipitating shallow cumulus convection. *Boundary-Layer Meteorology*, 163(3), 357–373. <https://doi.org/10.1007/s10546-016-0230-1>
- Schmidt, G. A., Ruedy, R., Hansen, J. E., Aleinov, I., Bell, N., Bauer, M., et al. (2006). Present-day atmospheric simulations using GISS ModelE: Comparison to in situ, satellite, and reanalysis data. *Journal of Climate*, 19(2), 153–192. <https://doi.org/10.1175/JCLI3612.1>
- Scinocca, J. F., McFarlane, N. A., Lazare, M., Li, J., & Plummer, D. (2008). Technical note: The CCCMA third generation AGCM and its extension into the middle atmosphere. *Atmospheric Chemistry and Physics*, 8(23), 7055–7074. <https://doi.org/10.5194/acp-8-7055-2008>
- Smith, R. N. B. (1990). A scheme for predicting layer clouds and their water content in a general circulation model. *Quarterly Journal of the Royal Meteorological Society*, 116(492), 435–460. <https://doi.org/10.1002/qj.49711649210>
- Sommeria, G., & Deardorff, J. W. (1977). Subgrid-scale condensation in models of nonprecipitating clouds. *Journal of the Atmospheric Sciences*, 34(2), 344–355. [https://doi.org/10.1175/1520-0469\(1977\)034<0344:SSCIMO>2.0.CO;2](https://doi.org/10.1175/1520-0469(1977)034<0344:SSCIMO>2.0.CO;2)
- Stephens, G. L., Vane, D. G., Boain, R. J., Mace, G. G., Sassen, K., Wang, Z., et al. (2002). The CloudSat mission and the A-train. *Bulletin of the American Meteorological Society*, 83(12), 1771–1790. <https://doi.org/10.1175/BAMS-83-12-1771>
- Stevens, B., Giorgetta, M., Esch, M., Mauritsen, T., Crueger, T., Rast, S., et al. (2013). Atmospheric component of the MPI-m earth system model: ECHAM6. *Journal of Advances in Modeling Earth Systems*, 5, 146–172. <https://doi.org/10.1002/jame.20015>
- Sundqvist, H., Berge, E., & Kristjánsson, J. E. (1989). Condensation and cloud parameterization studies with a mesoscale numerical weather prediction model. *Monthly Weather Review*, 117(8), 1641–1657. [https://doi.org/10.1175/1520-0493\(1989\)117<1641:CACPSW>2.0.CO;2](https://doi.org/10.1175/1520-0493(1989)117<1641:CACPSW>2.0.CO;2)
- Taylor, K. E. (2001). Summarizing multiple aspects of model performance in a single diagram. *Journal of Geophysical Research*, 106(D7), 7183–7192. <https://doi.org/10.1029/2000JD900719>
- Tiedtke, M. (1993). Representation of clouds in large-scale models. *Monthly Weather Review*, 121(11), 3040–3061. [https://doi.org/10.1175/1520-0493\(1993\)121<3040:ROCILS>2.0.CO;2](https://doi.org/10.1175/1520-0493(1993)121<3040:ROCILS>2.0.CO;2)
- Tompkins, A. (2005). *The parameterization of cloud cover* (Technical Memorandum). Reading, UK: European Center for Medium-Range Weather Forecasts. Retrieved from <https://www.ecmwf.int/sites/default/files/elibrary/2005/16958-parameterization-cloud-cover.pdf>
- Tompkins, A. M. (2002). A prognostic parameterization for the subgrid-scale variability of water vapor and clouds in large-scale models and its use to diagnose cloud cover. *Journal of the Atmospheric Sciences*, 59(12), 1917–1942. [https://doi.org/10.1175/1520-0469\(2002\)059<1917:APPFTS>2.0.CO;2](https://doi.org/10.1175/1520-0469(2002)059<1917:APPFTS>2.0.CO;2)
- Wang, S., O'Neill, L. W., Jiang, Q., de Szoeke, S. P., Hong, X., Jin, H., et al. (2011). A regional real-time forecast of marine boundary layers during VOCALS-REx. *Atmospheric Chemistry and Physics*, 11(2), 421–437. <https://doi.org/10.5194/acp-11-421-2011>
- Watanabe, M., Emori, S., Satoh, M., & Miura, H. (2009). A PDF-based hybrid prognostic cloud scheme for general circulation models. *Climate Dynamics*, 33(6), 795–816. <https://doi.org/10.1007/s00382-008-0489-0>
- Wood, R. (2012). Stratocumulus clouds. *Monthly Weather Review*, 140(8), 2373–2423. <https://doi.org/10.1175/MWR-D-11-00121.1>
- Wood, R., Mechoso, C. R., Bretherton, C. S., Weller, R. A., Huebert, B., Straneo, F., et al. (2011). The VAMOS ocean-cloud-atmosphere-land study regional experiment (VOCALS-REx): Goals, platforms, and field operations. *Atmospheric Chemistry and Physics*, 11(2), 627–654. <https://doi.org/10.5194/acp-11-627-2011>
- Wyant, M. C., Bretherton, C. S., Wood, R., Carmichael, G. R., Clarke, A., Fast, J., et al. (2015). Global and regional modeling of clouds and aerosols in the marine boundary layer during VOCALS: The VOCA Intercomparison. *Atmospheric Chemistry and Physics*, 15(1), 153–172. <https://doi.org/10.5194/acp-15-153-2015>
- Xiao, H., Mechoso, C. R., Sun, R., Han, J., Pan, H.-L., Park, S., et al. (2014). Diagnosis of the marine low cloud simulation in the NCAR community earth system model (CESM) and the NCEP global forecast system (GFS)-modular ocean model v4 (MOM4) coupled model. *Climate Dynamics*, 43(3), 737–752. <https://doi.org/10.1007/s00382-014-2067-y>
- Xie, S., Ma, H.-Y., Boyle, J. S., Klein, S. A., & Zhang, Y. (2012). On the correspondence between short- and long-time-scale systematic errors in CAM4/CAM5 for the year of tropical convection. *Journal of Climate*, 25(22), 7937–7955. <https://doi.org/10.1175/JCLI-D-12-00134.1>
- Zhang, M., Lin, W., Bretherton, C. S., Hack, J. J., & Rasch, P. J. (2003). A modified formulation of fractional stratiform condensation rate in the NCAR Community Atmosphere Model (CAM2). *Journal of Geophysical Research*, 108(D1), 4035. <https://doi.org/10.1029/2002JD002523>
- Zheng, X., Klein, S. A., Ma, H.-Y., Bogenschutz, P., Gettelman, A., & Larson, V. E. (2016). Assessment of marine boundary layer cloud simulations in the CAM with CLUBB and updated microphysics scheme based on ARM observations from the Azores. *Journal of Geophysical Research: Atmospheres*, 121, 8472–8492. <https://doi.org/10.1002/2016JD025274>